1   **Insight into glycosphingolipid crypticity: Crystal structure of the anti-**

2   **tumor antibody 14F7 and recognition of NeuGc GM3 ganglioside**

3

4   Kaare Bjerregaard-Andersen[1,8#], Hedda Johannesen[1,2#], Fana Abraha[3,8], Aleksandra

5   Šakanović[4], Daniel Großer[5,6], Ünal Coskun[5,6], Gregor Anderluh[4], Stefan Oscarson[3],

6   Ernesto Moreno[7]*, Michal Grzybek[5,6]*, Ute Krengel[1]*

7

8

9   [1] Department of Chemistry, University of Oslo, NO-0315 Oslo, Norway

10   [2] Department of Biosciences, University of Oslo, NO-0316 Oslo, Norway

11   [3] School of Chemistry, University College Dublin, Belfield, Dublin 4, Ireland

12   [4] Department of Molecular Biology and Nanobiotechnology, The National Institute of
13   Chemistry, 1000, Ljubljana, Slovenia

14   [5] Paul Langerhans Institute Dresden of the Helmholtz Zentrum Munich at the
15   University Hospital and Faculty of Medicine Carl Gustav Carus of Technische
16   Universität Dresden, Dresden, Germany

17   [6] German Center for Diabetes Research (DZD e.V.), Neuherberg, Germany

18   [7] Facultad de Ciencias Básicas, Universidad de Medellín, Medellín, Colombia

19   [8] Present addresses: Kaare Bjerregaard-Andersen, H. Lundbeck A/S, Valby,
20   Denmark; Fana Abraha, Recipharm OT Chemistry, Uppsala, Sweden

21

22   [#]Authors contributed equally

23   [*]Correspondence: Ernesto Moreno (emoreno@udem.edu.co); Michal Grzybek

24   (michal.grzybek@tu-dresden.de) and Ute Krengel (ute.krengel@kjemi.uio.no)

25

26

Abstract

Tumor-associated glycolipids such as NeuGc GM3 are auspicious molecular targets in antineoplastic therapies and vaccine strategies. 14F7 is an anti-tumor antibody with high clinical potential, which has extraordinary specificity for NeuGc GM3, but does not recognize the very similar, ubiquitous NeuAc GM3. Here we present the 2.3 Å crystal structure of the 14F7 binding domain (14F7 scFv) in complex with the NeuGc GM3 trisaccharide. Intriguingly, a water molecule appears to shape the specificity of 14F7. Using model membrane systems, we show that 14F7 recognizes NeuGc GM3 only above lipid concentrations that are likely to form glycolipid-rich domains. This "all-or-nothing" effect was exacerbated in giant unilamellar vesicles and multilamellar vesicles, whereas no binding was observed to 100 nm liposomes, emphasizing that the 14F7–NeuGc GM3 interaction is additionally modulated by membrane curvature. Unexpectedly, adding NeuAc GM3 strongly increased binding affinity to NeuGc GM3-containing liposomes. This effect may be important for tumor recognition, where the ubiquitous NeuAc GM3 may enhance 14F7 binding to NeuGc GM3-expressing cancer cells.

Introduction

Cancer cells differ from healthy cells by aberrant glycosylation patterns, displaying tumor-associated carbohydrate antigens (TACAs)[1-3]. Immunotherapy offers the possibility of specifically targeting TACAs with high affinity through structure-based engineering of monoclonal antibodies[4-6]. The monoclonal antibody (mAb) 14F7 is an IgG$_1$ raised by immunizing a BALB/c mouse with *N*-glycolyl GM3 (NeuGc GM3) complexed with very low-density lipoproteins (VLDLs)[7]. This antibody is known for its exquisite specificity and high affinity to NeuGc GM3, determined by ELISA to be in the low nanomolar range[7-9]. 14F7 has been used to verify the presence of the NeuGc GM3 in a range of tumors including retinoblastoma[10], non-small cell lung cancer[11], colon cancer[12], breast cancer[7,13] and melanoma[7]. Humanizing the mAb yielded 14F7hT (here referred to as 14F7 mAb), which retained its original ability to induce antibody-dependent cellular cytotoxicity in both human and murine NeuGc GM3-expressing cells[14,15]. 14F7 mAb has been reported to kill primary tumor cells by a complement-independent mechanism[16,17], however, the details of its mode of action are unknown.

The ability of 14F7 to effectively differentiate between the highly similar NeuGc and NeuAc epitopes is intriguing. In fact, the two glycolipids only differ by the presence of one additional oxygen atom (H to OH) present in NeuGc GM3 (Figure 1A). Mutational studies have highlighted key residues involved in NeuGc binding[18]. The structural basis of the discrimination between NeuGc and NeuAc GM3 has, however, remained elusive. Partial understanding has been gained through the crystal structure of the 14F7 Fab[19] and the more recent structure of a 14F7-derived single-chain variable fragment (scFv) harboring an alternative light chain[9]. Both 14F7 formats feature a long CDR H3 loop, which exhibits key residues for antigen binding.

NeuGc GM3 is composed of a ceramide tail, buried in the plasma membrane of the cell, and an exposed trisaccharide head group featuring the sialic acid NeuGc at its tip[20]. While NeuGc GM3 is expressed in most mammals, it is absent from healthy adult human cells due to a partial deletion in the cytidine monophosphate-*N*-acetylneuraminic acid hydroxylase (*CMAH*) gene converting NeuAc to NeuGc[21,22]. However, dietary uptake of NeuGc GM3, *e.g.*, from meat, can lead to low levels present in healthy tissue[23-27]. This in turn leads to a low level of autoantibodies, and NeuGc GM3 is therefore referred to as a xeno-autoantigen[28]. In contrast to NeuGc GM3, its *N*-acetyl counterpart is found ubiquitously in human cells and plays a role in control of

80   numerous cellular signaling pathways[29,30]. NeuAc GM3 has also been shown to interact

81   with integral membrane proteins, such as the insulin receptor[31], or the epidermal growth

82   factor receptor[32,33]. By mechanisms that are not yet well understood[23,28,34-37], NeuGc

83   GM3 is displayed to a larger extent by certain cancer cells and thus represents an

84   attractive TACA.

85   Here we present the X-ray crystal structure of the scFv–NeuGc complex, elucidating

86   the molecular basis for its discrimination between NeuAc and NeuGc GM3. Analysis

87   of the crystal structure has been expanded through molecular modeling to propose an

88   alternative binding mode of the GM3 lactose moiety that better explains previous

89   mutagenesis data. Furthermore, our binding experiments of the 14F7 mAb and scFv to

90   NeuGc GM3 reconstituted in liposomes show that the antibodies efficiently recognize

91   the ganglioside only at high concentrations. Interestingly, the presence of NeuAc GM3

92   potentiates antibody recognition of NeuGc GM3, suggesting that 14F7 mAb and scFv

93   can be potent tools for targeting low molar concentrations of the NeuGc GM3 antigen

94   in NeuAc GM3-expressing cells.

95

Results

Crystal structure of 14F7 scFv in complex with NeuGc GM3 trisaccharide

The structure of the 14F7 scFv in complex with the NeuGc GM3 trisaccharide was determined to 2.3 Å resolution from a single trisaccharide-soaked crystal. Data collection and refinement statistics are summarized in

Table 1. The crystal was obtained from the same batch of crystallization setups that earlier yielded the scFv apo-structure (PDB ID: 6FFJ[9]) and retained $P2_1$ symmetry upon soaking, with similar unit cell parameters and four scFv molecules in the asymmetric unit. Two of the four molecules (chains A and B) were well defined by electron density in the CDR regions and could be modeled without breaks, whereas parts of CDR H3 could not be traced in chains C and D. One of the molecules (chain A) contained additional electron density corresponding to the trisaccharide ligand (Figure 1B). Inspection of the ligand complex revealed that only the sialic acid component (NeuGc) of the trisaccharide interacts with the antibody (Figure 1C), whereas the glucose moiety extends outwards towards the solvent, where it makes contacts with residues of a neighboring scFv within the same crystallographic asymmetric unit. In this binding mode, the glycosidic linkage between NeuGc and Gal adopts a synclinal conformation[38].

Overall, the structure of the scFv−NeuGc GM3 trisaccharide complex is highly similar to the previously published scFv apo-structure[9], with an average r.m.s.d. value of 0.6 Å for Cα atoms indicating very little structural change upon binding (Figure 1B). Also, the side chain conformations of amino acid residues in proximity of the saccharide binding site are very similar between the scFv complex and the apo-structure. Tyr32 and Tyr100$_D$, both in direct contact with the ligand through H-bonds, shift by approximately 1 Å to accommodate binding. Most noticeably, Arg98 adopts a new conformation upon ligand binding, where it stacks against the sialic acid residue of the NeuGc GM3 trisaccharide (Figure 1C and D).
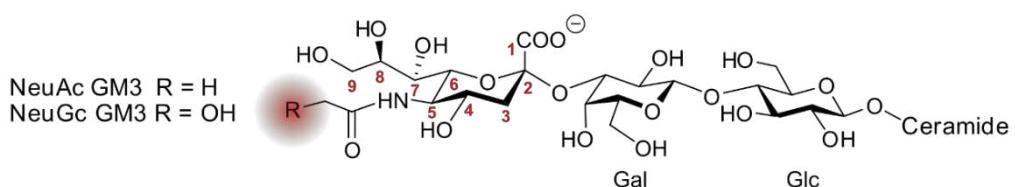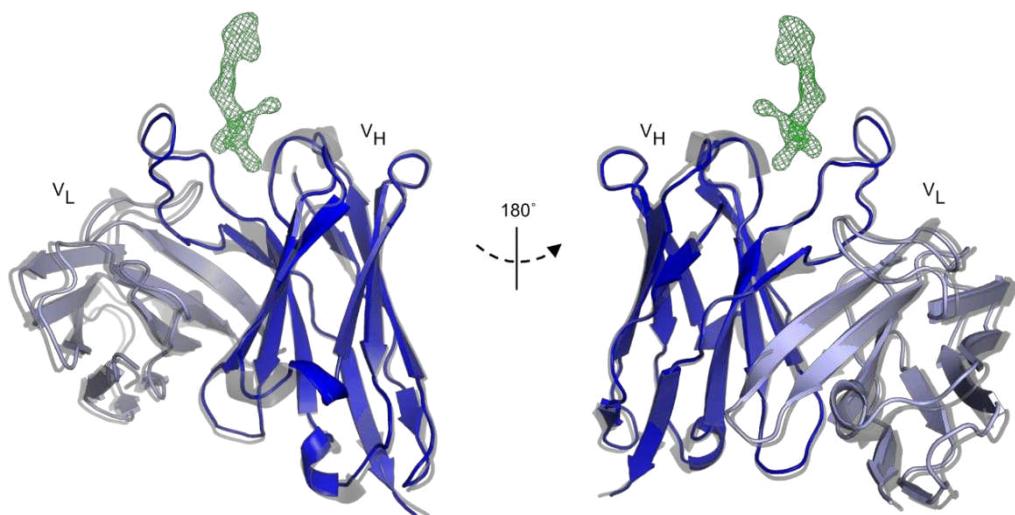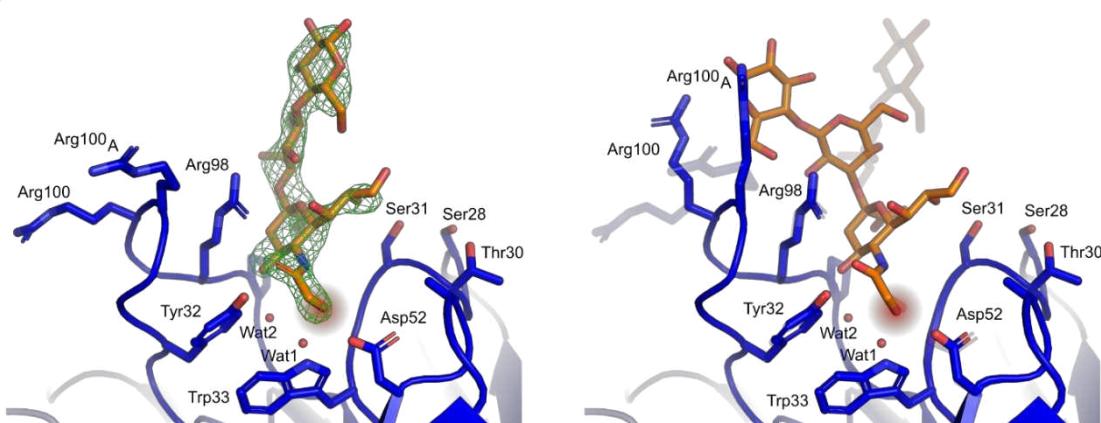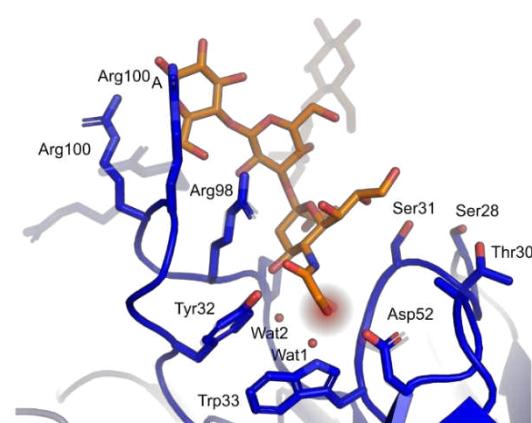
124

Figure 1. **14F7 scFv complex with NeuGc GM3 trisaccharide. A** Ganglioside structure. Neu5Gc GM3 is a xeno-antigen with a very similar structure to the common cellular glycolipid Neu5Ac GM3. The only difference consists of an additional oxygen atom in the *N*-glycolyl group of NeuGc compared to the *N*-acetyl group of NeuAc (highlighted in salmon) in the context of the trisaccharide Neuα2-3Galβ1-4Glcβ. **B** 14F7 scFv light (light blue) and heavy (dark blue) chains (PDB ID: 6S2I, chain A; this work). The 14F7 scFv apo-structure (PDB ID: 6FFJ[9], chain A) is superimposed in grey. Difference electron density (mF_o-DF_c) for the carbohydrate ligand is shown at 3.0 σ (green mesh). **C** Structural model of 14F7scFv—NeuGc trisaccharide complex (synclinal conformation). Key amino acid residues and water molecules interacting with the glycan (orange) are labeled. **D** Alternative conformation of NeuGc GM3 trisaccharide with anticlinal glycosidic linkage between NeuGc and Gal (modeled), which buries a larger surface area on 14F7 scFv compared to the synclinal conformation observed in the crystal structure (transparent). Panel A was prepared with ChemDraw, panels B-D with PyMOL 2.2.0.

Table 1. Crystallographic data collection and refinement statistics

| 14F7 scFv – NeuGc complex (PDB ID: 6S2I)*			
Data collection		**Refinement**	
Beam line	ID30A-3, ESRF	Resolution (Å)	62.9-2.29 (2.34-2.29)
Wave length (Å)	0.9677	No. unique reflections	42066 (2675)
Space group	$P\,2_1$	No. reflections in test set	2151 (126)
Unit cell parameters		*R*-work / *R*-free	0.220 / 0.255
a, b, c (Å)	63.9 113.7 67.0	No. atoms	
α, β, γ (°)	90 91.2 90	Protein	7239
Solvent content (%)	51.0	Water	103
Resolution (Å)	62.9-2.29 (2.34-2.29)**	Ligand	44
R_{sym} (%)	9.7 (69.7)	*B*-factors (Å^2)	
R_{meas} (%)	11.1 (76.8)	Protein	52.1
$I / \sigma(I)$	9.3 (2.1)	Water	48.6
Completeness (%)	98.8 (99.2)	Ligand	52.0
Multiplicity	4.2 (4.4)	R.m.s. deviations	
CC 1/2	0.99 (0.83)	Bond lengths (Å)	0.002
Wilson *B*-factor (Å^2)	44.0	Bond angles (°)	0.6
		Ramachandran plot	
		Favored (%)	97.3
		Allowed (%)	2.7
		Outliers (%)	0.0

125 *Data collected on a single crystal.
126 **Values in parentheses are for high-resolution shell.

Structural basis for 14F7 discrimination between NeuGc and NeuAc GM3

The interactions between 14F7 and the NeuGc GM3 trisaccharide are shown in Figure 2A and listed in Table 2. 14F7 has repeatedly been shown to strongly differentiate between NeuGc and NeuAc GM3 *in vitro*, *e.g.*, probed by ELISA[7,9]. Therefore, the key determinant for discrimination must be found in the trisaccharide head group, where the only difference is the presence of an additional hydroxyl group in the *N*-glycolyl moiety of the sialic acid. Intriguingly, the *N*-glycolyl hydroxyl group does not itself provide any direct interaction with the scFv, except for a backbone interaction with Tyr32, but manifests its presence through a water molecule (Wat1; Figure 2A). Wat1 is part of a hydrated pocket coordinated by Trp33 and is also present in the 14F7 scFv apo-structure (PDB ID: 6FFJ[9]), thus it may be regarded as an extension of CDR H1. Wat1 not only interacts with the *N*-glycolyl hydroxyl group of NeuGc, but also with its 4-OH group, *via* a second water molecule (Wat2), which binds to the backbone oxygen of Ser96. On the protein side, Wat1 establishes an H-bond with the backbone NH of Trp33 and a weaker, out-of-plane H-bond with the aromatic π face of its indole pyrrole ring. Mutagenesis of Trp33 reveals that specificity is only maintained when this residue is exchanged by another aromatic residue, *i.e.*, Phe and Tyr[18].

144   Especially the possible replacement by Phe emphasizes the importance of the aromatic

145   interaction with Wat1. This trisaccharide-water complex, unable to form with NeuAc,

146   places itself like a cassette into the bottom of the binding pocket formed by the

147   backbone and side chains of Ser31, Tyr32, Pro97, Arg98 and Tyr100$_D$. The difference

148   in energetic contribution to binding of this exciting water-mediated ligand binding site

149   remains to be explored.
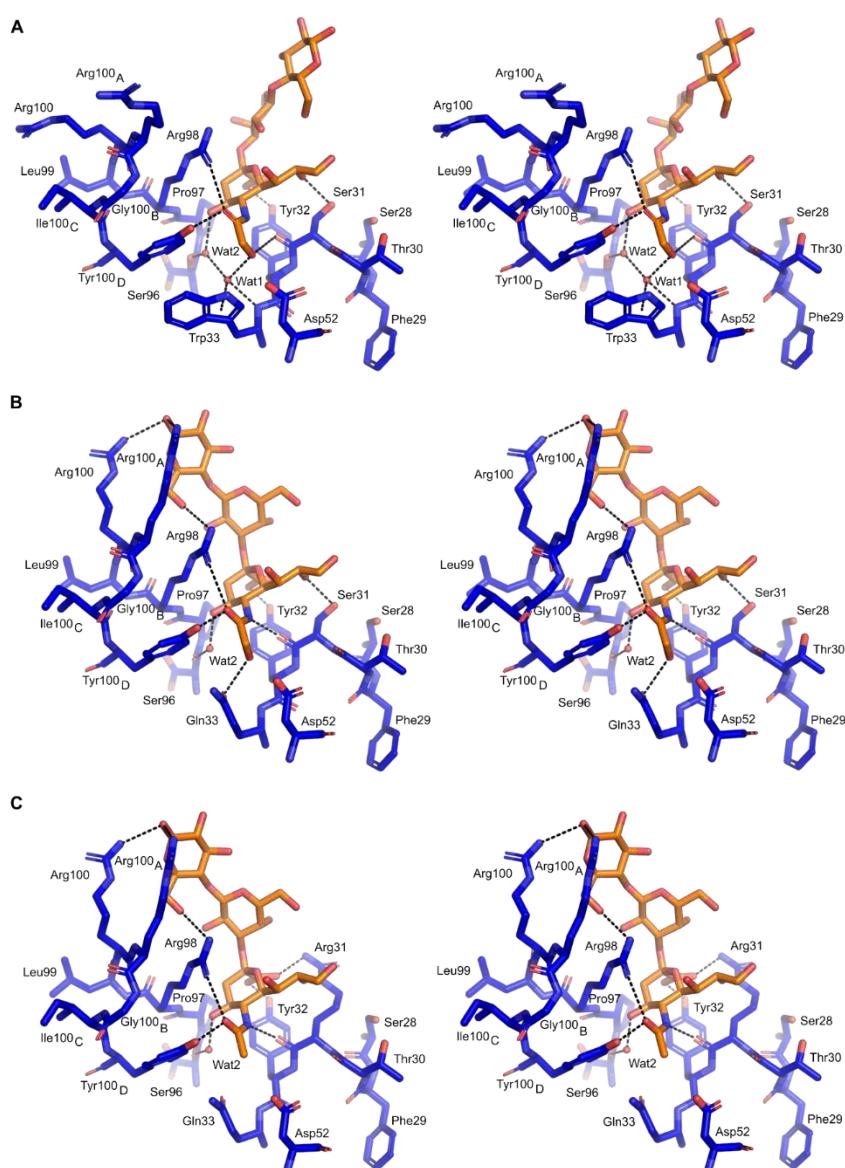
150

Figure 2. **Stereo pictures showing the specificity of Trp33, W33Q and W33Q/S31R 14F7 variants in complex with NeuGc or NeuAc. A** Crystal structure of 14F7 Trp33 (blue) bound to NeuGc (orange) in its experimentally determined conformation (PDB ID: 6S2I, chain A; this work). **B** Model of 14F7 W33Q variant, with NeuGc in the *in silico*-optimized anticlinal conformation. **C** Model of the cross-reactive 14F7 S31R/W33Q variant, with NeuAc in the anticlinal conformation. The figure was prepared with PyMOL 2.0.0.

Table 2. Protein-carbohydrate interactions.

Synclinal (crystal) conformation			Anticlinal (modeled) conformation		
Sugar Residue-Atom	Protein Amino acid-Atom [a]	Dist. (Å)	Sugar Residue-Atom	Protein Amino acid-Atom [a]	Dist. (Å)
SIA-O1A	Tyr32-OH	2.5			
SIA-O1A	Pro97-CB	3.4			
SIA-O1B	Tyr32-OH	3.1			
SIA-C3	Tyr32-CE1	4.4			
SIA-C3	Arg98-NE	4.0			
SIA-C4	Tyr32-CD1	4.2			
SIA-O4	Wat2	2.4			
SIA-O4	Arg98-N	2.9			
SIA-O4	Arg98-CG	3.4			
SIA-O4	Arg98-CD	3.4			
SIA-C5	Arg98-CZ	4.5	*Idem*		
SIA-N5	Ser31-O	2.8			
SIA-O5	Tyr100$_D$-OH	2.6			
SIA-C5A	Tyr100$_D$-CE1	3.6			
SIA-OGc	Wat1	2.4			
SIA-OGc	Ser31-O	3.4			
SIA-OGc	Trp33-NE1	3.3			
SIA-OGc	Tyr32-CA	3.7			
SIA-C6	Ser31-O	3.3			
SIA-C7	Ser31-CB	4.4			
SIA-C7	Ser31-CG	4.4			
SIA-O8	Ser31-OG	2.8			
SIA-O8	Arg23-NH1 #	2.9	Crystal contact not relevant		
SIA-O5	Arg98-NH1	3.2	SIA-O5	Arg98-NH1	2.7
			SIA-O7	Arg98-NH1	3.1
			GAL-O1	Arg100$_A$-NH2	2.9
			GAL-O2	Arg98-NE	4.1
			GAL-O5	Arg100$_A$-NE	3.6
			GLC-O1	Arg100-NH2	3.2
Absent			GLC-O5	Arg100-NE	3.8
			GLC-C6	Arg100-CG	4.1
			GLC-O6	Arg98-NH2	3.5
			GLC-O6	Arg98-NE	3.7
			GLC-O6	Arg100$_A$-CG	3.6
			GLC-O6	Arg100$_A$-N	4.1
GLC-O1	Ser74-O #	2.5	Crystal contacts not relevant		
GLC-O5	Asn76-ND2 #	3.3			
Buried protein surface [b]					
218 Å^2			293 Å^2		

151   Atomic contacts between sugar and protein/water atoms for the synclinal (crystal) and anticlinal
152   (modeled) conformations, defined by the sialic acid-galacto*se glycosidic linkage.* Packing contacts with
153   distances up to 4.5 Å were also included in the table. Contacting carbon atoms are shaded in light gray.
154   [a] Amino acid atom names follow PDB conventions, # marks a neighboring molecule in the crystal.
155   [b] In these calculations, the two buried waters were considered part of the protein. The contribution of the
156   neighboring chain (#), due to crystal packing, was not included in the calculations.

157

158

Alternative trisaccharide binding mode

In the crystal, NeuGc GM3 adopts synclinal torsion angles between NeuGc and Gal. In solution, a common alternative conformation of the NeuGc GM3 trisaccharide has an anticlinal glycosidic linkage. Reasoning that crystal packing might have forced the orientation of the lactose moiety of NeuGc GM3 into the conformation observed in the crystal structure, we modeled an alternative binding mode for the trisaccharide, where NeuGc remained exactly as in the crystal structure, but the two torsion angles of its glycosidic linkage with galactose adopt the anticlinal conformation (Figure 1D). We found that this binding geometry, which is hindered by the crystal packing, brings additional favorable contacts between the trisaccharide and CDR-H3, including interactions between both Arg100 and Arg100$_A$ with the trisaccharide glucose residue (Table 2). It also increases the buried surface area by more than one third, from 218 Å^2 to 293 Å^2. Furthermore, in this binding mode, Arg98 becomes more tightly packed against the trisaccharide (Figure 1D, Figure 2AB). This is in good agreement with mutagenesis data showing the critical role of this amino acid, which did not tolerate any substitution[18].

Models of 14F7 variants explore functional mapping data

In previous work, we used phage display to perform extensive mutagenesis studies on the 14F7 heavy chain CDRs[18]. These studies identified several positions in CDRs H1 and H3 as important for recognizing NeuGc GM3, *e.g.* Trp33, Asp52, Arg98, Arg100, Arg100$_A$ and Tyr100$_D$. In addition we found that several single residue substitutions, yielding *e.g.*, S28R, T30R, S31R and W33Q conferred different levels of cross-reactivity to the antibody; and some double or triple combinations even raised the affinity to NeuAc GM3 to the same level as for NeuGc GM3[18]. Here we modeled one of these variants (W33Q) in complex with NeuGc GM3 (Figure 2B) and another (S31R/W33Q) in complex with NeuAc GM3 (Figure 2C), in order to interpret the mutagenesis data. The introduction of an arginine residue in the antigen binding site is likely to yield a salt bridge with the sialic acid carboxylate. Gln33 (as in W33Q) probably interacts directly with the *N*-glycolyl OH of NeuGc GM3, replacing Wat1 (Figure 2B).

191   **14F7 binding to NeuGc GM3 occurs only at high glycolipid densities**

192   To better understand the mode of interaction between 14F7 and NeuGc GM3 in the

193   lipid bilayer, we performed a series of binding experiments using different model

194   membrane systems. First, we chemically labeled 14F7 mAb and scFv with fluorescent

195   dyes and tested their binding to giant unilamellar vesicles (GUVs) containing various

196   amounts of NeuGc or NeuAc GM3 in a background of DOPC and cholesterol

197   (Figure 3). Below 2 % NeuGc GM3, no binding to GUVs was detected. Even upon

198   increasing the glycolipid concentration from 2 % to 5 % NeuGc GM3, only ~3 % of all

199   vesicles showed antibody binding. However, when 10 % NeuGc GM3 was used for

200   GUV formation, all vesicles were labeled (Figure 3), suggesting that 14F7 mAb is not

201   capable of recognizing individual NeuGc GM3 glycolipids as antigens. Upon

202   surpassing a critical glycolipid density threshold, however, antigen recognition

203   becomes highly efficient. In contrast, no binding was observed for 10 % NeuAc,

204   confirming the specificity of 14F7 (Figure 3).

205
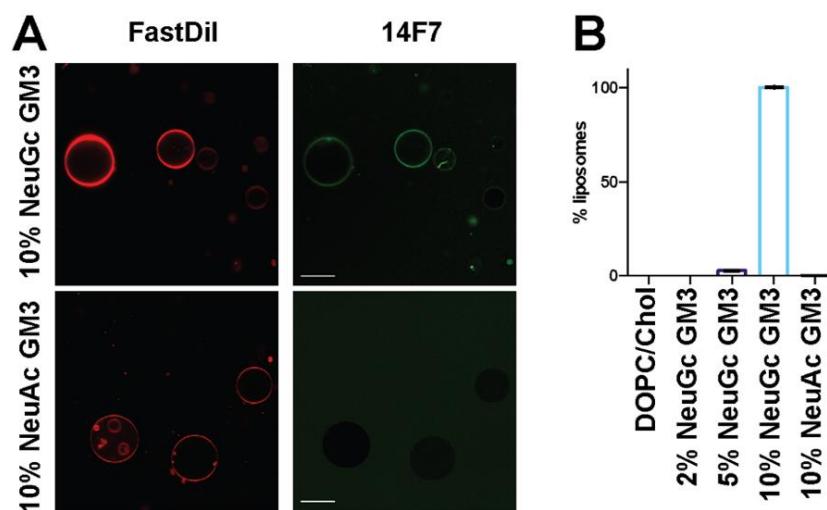
206

207   *Figure 3*. **Binding of 14F7 to GUVs composed of DOPC/Chol/GM3. a**14F7 was chemically
208   labeled with Dylight-488 (green) and was added to GUVs containing FastDiI as a membrane
209   marker (red). The scale bar corresponds to 20 μm. **b** Percentage of GUVs showing binding of
210   14F7-488. Representative images for all lipid compositions are shown in Figure S1.

211

212   The experiment was repeated with fluorescently labeled 14F7 scFv instead of 14F7

213   mAb, however, no binding was observed, even at high NeuGc concentrations. To test

214   whether this failure in binding was related to loss of function in the 14F7 scFv or an

215   artifact of chemical labeling, we performed differential-scanning calorimetry

216   (nanoDSF) of the unlabeled and labeled scFv fragment (Figure S3). After chemical

217   labeling with Dylight488-NHS, the T_m of 67 °C for the native 14F7 scFv flattened and

218   shifted its maximum to 72 °C (Figure S3). In addition, the scattering of the solution

219   increased substantially, suggesting that the sample becomes polydisperse. Both of these

220   results indicate an overall change in the structure of the scFv upon labeling that

221   probably also perturbs the binding site. We therefore opted for liposomal flotation

222   experiments that do not require labeling of the protein.

223

224   **Membrane curvature can affect NeuGc GM3 presentation**

225   To test if both 14F7 mAb and scFv can recognize NeuGc GM3-containing liposomes,

226   we performed flotation assays with unlabeled protein. Large unilamellar vesicles

227   (LUVs) have an advantage over GUVs in that they form more homogenous liposome

228   populations due to their preparation method, using freeze-thaw cycles, followed by

229   multiple extrusions through polycarbonate filters. After the flotation assay, the

230   gradients were fractionated from top to bottom, and binding of 14F7 to vesicles was

231   detected by Western blotting. Antibody binding to LUVs is indicated by its presence in

232   the top, low-density fractions (fractions 2-4), otherwise, the protein would be pelleted

233   at the bottom (fractions 10-11) (Figure 4A). In the initial experiment, LUVs containing

234   10 % NeuGc GM3 were used, but only a small portion of either 14F7 mAb or scFv was

235   detected in the liposome-containing fractions, suggesting a very weak interaction with

236   the LUVs (Figure 4BC). Thin layer chromatography (TLC) analysis of the liposomes

237   recovered after flotation confirmed the presence of NeuGc GM3 in the vesicles, thus

238   the weak binding was puzzling. The major difference between the LUVs and the

239   liposomes used in the fluorescent study (GUVs) was their size (Figure 4D). Therefore,

240   we repeated the flotation experiment using non-extruded, multilamellar liposomes

241   (MLVs), which correspond in size to the GUVs. Interestingly, strong binding for both

242   14F7 mAb and scFv was observed for the MLVs, suggesting that membrane curvature

243   plays an important role for antigen recognition (Figure 4BC). A comparative analysis

244   of lipid composition of both LUVs and MLVs confirmed that in both cases the

245   composition of the vesicles was the same (Figure 4E). In fact, the amount of NeuGc

246   GM3 that was available for binding should be much higher in LUVs than in MLVs, as

247   only the outermost membrane leaflet can be probed by the antibodies. When NeuAc

248   GM3 was used in either LUVs or MLVs, no binding was observed, neither for 14F7

249   mAb nor for scFv, again confirming the high specificity of 14F7 (Figure S2).
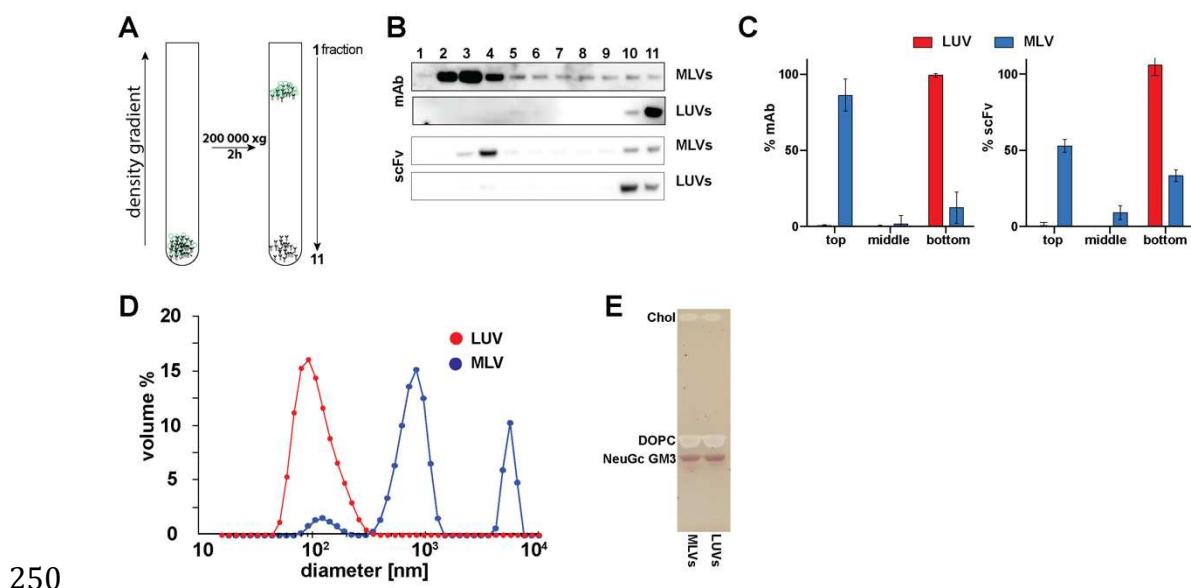
250

Figure 4. **Binding of 14F7 to LUVs and MLVs composed of DOPC/Chol/NeuGc GM3 in flotation assays. A** Setup of the LUV flotation assay. After the centrifugation, 11 fractions were collected from the top. Proteins bound to vesicles accumulate in fractions 2-4, while unbound proteins are in the bottom fractions (10-11) **B** Representative Western blot of fractions collected after flotation. **C** Binding was quantified using the AIDA software as follows: top (fractions 1-4), middle (5-8) and bottom (9-11). Error bars represent standard deviations of three independent experiments. **D** Dynamic light-scattering measurement of the size of the vesicles used in the flotation assay. **E** Thin layer chromatography (TLC) of lipids extracted from the vesicles after flotation (combined fractions 2-4). The lipids were stained with orcinol.

251   **NeuAc GM3 potentiates 14F7 binding to NeuGc GM3**

252   We decided to probe 14F7 mAb and scFv binding to MLVs containing various NeuGc

253   GM3 concentrations (0-10 %) by electrochemiluminescence immunoassay (EIA), and

254   also tested combinations of NeuGc and NeuAc GM3. The K_D values for vesicles

255   containing 10 % NeuGc GM3 were estimated to be approximately 34 nM and 3.4 μM

256   for 14F7 mAb and scFv, respectively by EIA (Figure 5AB), representing a large gain

257   in apparent affinity (approximately 100-fold) for the mAb *versus* the scFv, in contrast

258   to the previous ELISA studies[8,9]. Interestingly, NeuGc GM3 binding and recognition

259   by 14F7 greatly increased when NeuAc GM3 was introduced into the same vesicles,

260   *e.g.*, binding of both 14F7 mAb and scFv to liposomes containing a mixture of 2 %

261   NeuGc and 8 % NeuAc GM3 was significantly higher compared to liposomes

262   containing only 2 % NeuGc. In fact, 14F7 scFv bound equally strongly to vesicles

263   containing 5 % NeuGc or a 2/8 % mixture of NeuGc and NeuAc GM3. For 14F7 mAb,

264   binding to the 2/8 % mixture even exceeded the binding efficiency observed for vesicles

265   containing 5 % pure NeuGc GM3. This effect of potentiation was also observed for

266   liposomes containing an equal molar ratio of NeuGc/NeuAc GM3 (5/5 %), which

267   showed higher binding efficiency compared to vesicles that only contained 5 %

268   NeuGc GM3 (Figure 5AB). Similar results were obtained by surface plasmon

269   resonance (SPR) spectroscopy (Figure 5C). This demonstrates that not only the amount

270   of NeuGc GM3, but also the overall GM3 ganglioside concentration affects the ability

271   of 14F7 to recognize and bind NeuGc GM3.

272
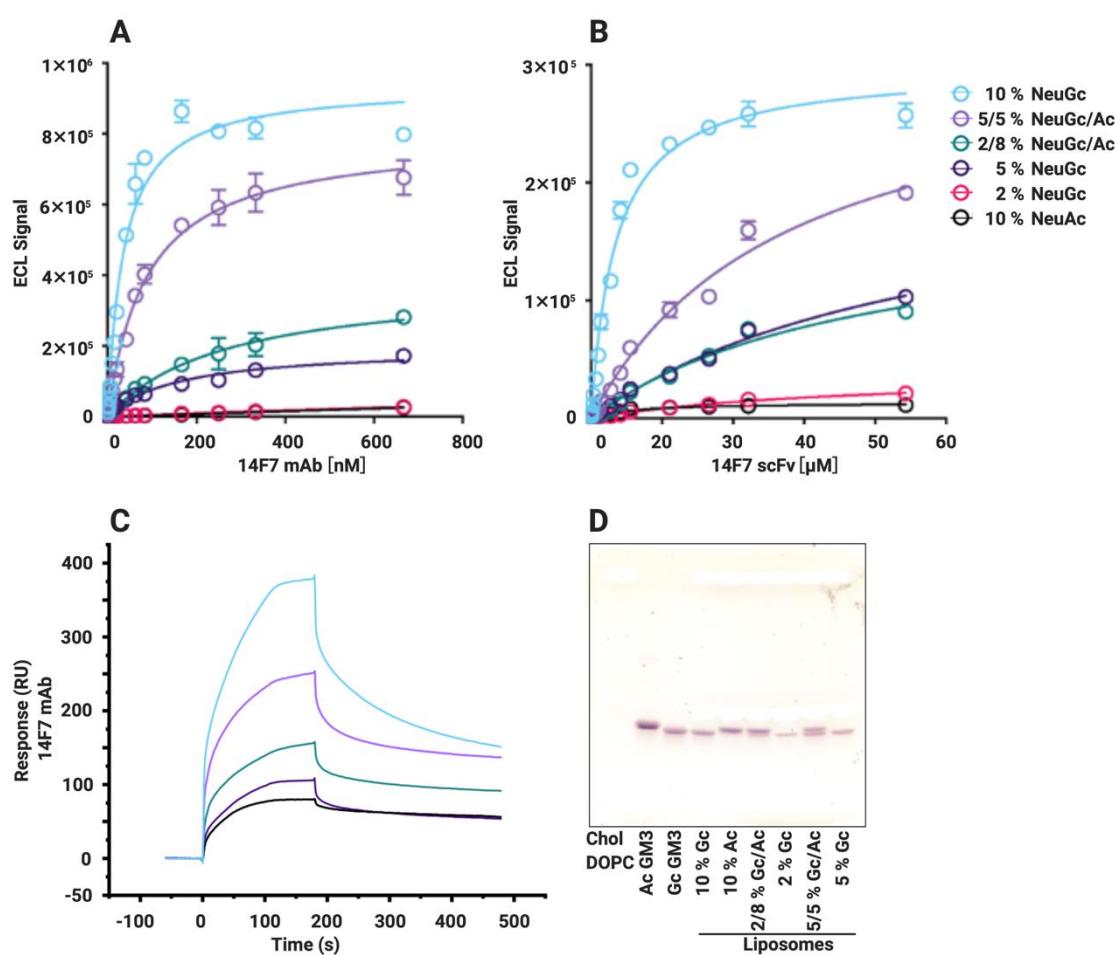
273

Figure 5. **Addition of NeuAc GM3 increases binding efficiency of 14F7 to NeuGc GM3.** Binding of (**A**) 14F7 mAb and (**B**) 14F7 scFv to MLVs composed of DOPC/Chol/GM3 measured by EIA. Representative plots of 3 independent measurements. **C** SPR spectroscopy of 14F7 mAb binding to an HPA chip with a monolayer of DOPC/Chol/GM3. The sensorgram represents one of two independent measurements (to save scarce sample), resulting in the same trend observed by EIA. **D** Thin layer chromatography of lipids extracted from the vesicles used in EIA assay. NeuAc and NeuGc GM3 were abbreviated Ac and Gc, respectively. The lipids were stained with orcinol.

Discussion

Gangliosides are sialic-acid containing glycosphingolipids present in the plasma membranes of all vertebrates. Together with cholesterol, sphingomyelin and specific membrane proteins, they are concentrated in membrane nanodomains often referred to as lipid rafts[39-45]. Gangliosides are functionally important and are known to modulate cellular signaling[46-49]. Despite decades of studies, the structure and function of these cell surface antigens remain to be fully appreciated, and only few anti-ganglioside antibodies have been raised[50].

14F7 specificity

14F7 can distinguish the very small chemical difference between the gangliosides NeuGc and NeuAc GM3[7,9], and even more remarkably, we have now discovered that it does so indirectly, through a water molecule. NeuGc GM3 engages in two water-mediated interactions with Trp33, one with its main chain and one with the π-system of the indole side chain (both through Wat1; Figure 2A). Such an interaction is weaker than an ordinary hydrogen bond[51], however, the importance of this interaction is highlighted by the fact that substitution of Trp33 with Phe or Tyr maintains specificity, while non-aromatic residues abolish binding or allow cross-reactivity with NeuAc GM3[18]. H-bonds commonly mediate specificity in antibody-antigen recognition through direct contact between paratope and epitope side chains[52]. In the case of 14F7, Wat1 is already present in the protein apo-structure (PDB ID: 6FFJ[9]). A thorough analysis of water–tryptophan interactions indicates that the six-membered ring of the indole side chain favors π-OH interaction, while the five-membered pyrrole ring favors π-lone pair interaction[53]. The latter appears to be the case for Wat1, thus positioning it as an H-bond donor for the *N*-glycolyl group of NeuGc GM3. While it is well known that the hydration shell is important for protein structure and function[54,55], including the recognition of carbohydrates[56-58] and antibody-antigen interactions[59-62], the complexity of antibody engineering is highlighted by our finding of this indirect, water-mediated specificity.

305 **Selectivity *versus* cross-reactivity**

306 NeuGc is bound to the bottom of a cleft formed by the variable heavy chain of 14F7

307 (Figure 2A), which is separated from the variable light chain through the long CDR H3

308 loop. The predicted NeuGc recognition site has previously been functionally mapped

309 by a combinatorial phage display strategy using an alternative format of 14F7 scFv[18].

310 The study revealed that substitution of Trp33 in combination with residues 28, 30 or 31

311 could yield cross-reactive 14F7 variants (*e.g.*, S28R/S30R/W33Q, S31R/W33Q and

312 S28R/S31R, and to a lesser extent by single amino acid substitutions)[18]. Therefore

313 cross-reactivity is likely mediated through direct interactions with the sialic acid

314 residue, in particular by a salt-bridge to the negatively charged carboxylate group found

315 in both NeuGc and NeuAc GM3. To further explore the mutagenesis data, we modeled

316 the 14F7 S31R/W33Q variant in complex with NeuAc GM3 (Figure 2C). Substituting

317 Trp33 as in 14F7 W33Q likely leads to the replacement of Wat1 by the glutamine side

318 chain amide, which can interact directly with the *N*-glycolyl OH of NeuGc GM3

319 (Figure 2B). This mutation alone decreased NeuGc GM3 binding, but promoted a weak

320 interaction to the NeuAc variant of GM3[18]. Substitution of Ser31 with Arg (S31R)

321 probably trades an H-bond to one of the NeuGc glycerol hydroxyls for a charge

322 interaction of the guanidinium moiety with the sialic acid carboxyl group found in both

323 NeuGc and NeuAc GM3 (Figure 2C), thus conferring some cross-reactivity to the

324 antibody. Arginine substitutions of Ser28 (S28R) or Thr30 (T30R) likely elicit similar

325 effects. Interestingly, in spite of this additional interaction, substituting Ser31 for Arg,

326 either alone or combined with other amino acid substitutions, hardly increased the

327 affinity for NeuGc GM3[18].

328 Although it may seem counterintuitive that NeuAc could bind to a polar pocket, a polar

329 environment is not unprecedented for NeuAc. For example, cross-reactive rotaviruses

330 that recognize both NeuAc and NeuGc GM3 have been shown to display similar polar,

331 water-containing pockets to accommodate the acetyl or glycolyl groups of their glycan

332 receptors[63]. Favorable interactions elsewhere, *e.g.*, with the sialic acid carboxylate or

333 glycerol chain, may well compensate for less favorable interactions of the *N*-acetyl

334 group. In fact, it is likely that selectivity of NeuGc over NeuAc GM3 requires a fine

335 balance of interactions, and that too tight binding of the sialic acid residue may prevent

336 selectivity and would tip the balance towards cross-reactivity towards NeuGc and

337 NeuAc GM3.

Glycan conformation and antibody recognition

In the crystal structure of the scFv–saccharide complex (PDB ID: 6S2I; this work), the saccharide adopts a synclinal conformation (Figure 1C), and the only interaction with 14F7 is *via* the sialic acid (Figure 2A). However, the carbohydrate conformation may be forced by the crystal, into which the ligand was soaked. For example, we note that the anticlinal conformation would lead to clashes with other protein molecules in the crystal, whereas the synclinal conformation is stabilized by an interaction of the sialic acid glycerol chain with V_L residue Arg23 of a neighboring scFv in the crystal (Table 2). In a biological context (and in solution), the saccharide would be free to adopt both conformations (Figure 1D) – also the anticlinal conformation, which provides a larger contact surface with the antibody (293 *versus* 218 $Å^2$). Dynamic binding may in fact provide an entropic advantage. In both conformations, the glycosidic linkage between NeuGc and Gal places the key CDR H3 residue Arg98 in a central position for interaction with the NeuGc GM3 trisaccharide (Figure 2AB), explaining why any substitution of this residue renders it incompatible with binding. In anticlinal conformation, Arg98 can additionally interact with the glucose moiety of NeuGc GM3 through H-bonds. This is also true for Arg100 and Arg100$_A$, which are located at the tip of CDR-H3. Moreover, the arginine residues exposed on CDR H3 create a strongly positively charged surface patch that will likely also interact with other components of the plasma membrane. The observation that these residues, in general, can be exchanged while maintaining a positive charge[18], indicate non-specific interactions with the membrane through negative charges found in the proximity of the target antigen, such as other phospholipids, gangliosides or proteins.

14F7–membrane interactions: "All-or-nothing" effect

To better understand the mode of interaction between the 14F7 and NeuGc GM3 in the context of a membrane, we performed binding measurements using different membrane-mimetic systems. These studies confirmed the selectivity of 14F7. However, binding was only observed above a concentration threshold of the NeuGc GM3 (Figure 3B). The observed "all-or-nothing" effect for glycolipid recognition is not a new concept in itself. For example, Nores *et al.* observed that the murine mAb M2590 only recognized the GM3 antigen when the ganglioside concentration in a membrane

370   reached a threshold of 8 %, as determined by binding to liposomes[64]. That 14F7 mAb

371   recognizes NeuGc GM3 in a similar manner is intriguing and suggests that at low

372   concentrations, the antigen remains "cryptic". For mAbs, avidity immediately springs

373   to mind as logical explanation for such a threshold effect, *i.e.*, if recognition by both

374   Fabs is required to detect and enhance binding. However, since the same effect is also

375   observed for the 14F7 scFv, both related to density and curvature, this clearly indicates

376   that avidity cannot be the main cause of the observed effect. Instead, it suggests that at

377   low concentrations, the glycolipid conformation in the membrane does not allow

378   recognition by the antibody (Figure 6A). At high concentrations, the gangliosides may

379   pack differently, for example through carbohydrate stacking[65], and expose their *N*-

380   glycolyl group to enable recognition (Figure 6B). The surrounding sialic acid residues

381   from other GM3 molecules close-by may further enhance affinity due to the increased

382   negative charge. The fact that the addition of NeuAc GM3 to low concentrations of

383   NeuGc GM3 enables and enhances 14F7 binding (Figure 5), supports this hypothesis.

384

NeuGc GM3 clustering

386   In contrast to the receptor-binding B-pentamer of the cholera toxin (CTB), which is

387   commonly used to label GM1 molecules and can lead to ganglioside clustering[66], 14F7

388   appears to bind only to pre-existing NeuGc GM3 assemblies and not drive the

389   formation of such. This conclusion is based on the observation that (i) the monovalent

390   scFv fragment showed similar binding characteristics as the mAb, and (ii) we never

391   observed any domain formation in GUVs, even after overnight incubation with the

392   divalent 14F7 mAb. For CTB, domain formation was observed when the protein was

393   incubated with GUVs containing substantially lower amounts of its main glycolipid

394   receptor, GM1[66].

395

Curvature effect

397   The collective behavior of lipids and physicochemical membrane properties can be

398   directly modulated by temperature, pressure and molecular stress[67,68]. Another

399   important parameter is membrane curvature[49,69-71]. Unexpectedly, we observed that the

400   anti-tumor antibody 14F7 preferentially recognizes NeuGc GM3 present in GUVs or

401   MLVs, but not in 100 nm LUVs. We hypothesize that high positive curvature might

402   disrupt carbohydrate stacking interactions critical for exposure of the NeuGc *N*-glycolyl

403   group, preventing NeuGc GM3 recognition as illustrated in Figure 6C.

404

405
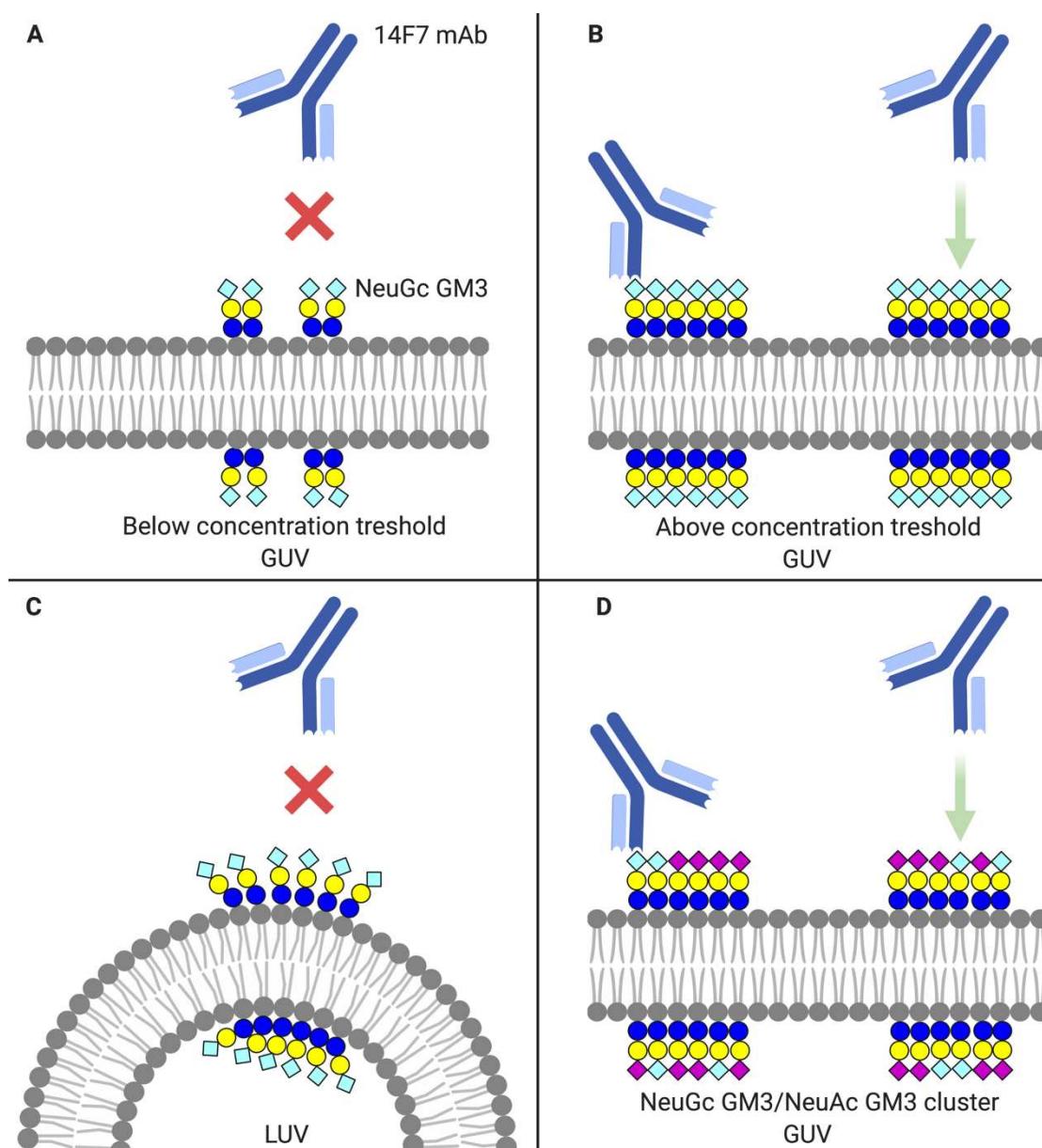
Figure 6. **Model of NeuGc GM3 recognition by 14F7**. **A** 14F7 binding is not observed at low NeuGc GM3 concentrations. **B** Above a ganglioside concentration threshold, 14F7 attaches to NeuGc GM3-containing glycolipid clusters on low-curvature membrane surfaces (GUV). **C** 14F7 does not bind to NeuGc GM3 in highly curved LUVs. **D** The addition of NeuAc GM3 to NeuGc GM3-containing liposomes enables 14F7 binding even at low NeuGc GM3 concentrations, possibly through the formation of functional glycolipid clusters. Carbohydrate symbols follow the nomenclature of the Consortium for Functional Glycomics: *N*-acetyl neuraminic acid – purple diamond; *N*-glycolyl neuraminic acid – light blue diamond; galactose – yellow circle; glucose – blue circle. Prepared with BioRender.

406

407   Many lipids have a cone shape rather than a cylindrical shape[72]. In a flat lipid bilayer,

408   the packing of cone-shaped lipids leads to packing tension (line-tension) that can be

409   relieved by the spontaneous formation of higher-order submicron clusters[69,70]. This

410   could be the driving force for NeuGc GM3 clustering, where ganglioside and

411   cholesterol form liquid-ordered structures surrounded by liquid-disordered regions[73,74].

412   It would be interesting to test if also negatively curved interfaces (*e.g.*, caveola and

413   endocytic pits) elicit the preferable conformation for 14F7 recognition.

414

415   **New applications for 14F7?**

416   In biological membranes, gangliosides are found in conjunction with cholesterol,

417   sphingomyelin and specific membrane proteins. Cholesterol is well known to modulate

418   glycolipid conformation and enable receptor binding[42,75-79]. Here, we show that also the

419   interaction between different gangliosides (*i.e.*, NeuAc and NeuGc GM3, Figure 6D)

420   can influence the conformation of glycolipids in the membrane – and make the

421   gangliosides amenable to recognition by 14F7. This is valuable information, for two

422   reasons: For one, it allows the detection of NeuGc GM3 even at low concentrations.

423   This is the case in human cells (and although NeuGc GM3 content appears to increase

424   in certain cancers, it is unclear if high concentrations can be reached). In contrast, the

425   non-binding NeuAc GM3 is naturally expressed in all cells and may thus potentiate the

426   recognition of low concentrations of NeuGc GM3 in cellular membranes, exposing the

427   antigen for specific targeting. So far, we have only studied 14F7's capacity to recognize

428   NeuGc GM3 clusters in a membrane mimetic system, however, it is reasonable to

429   assume that a similar effect occurs in a cellular environment. Although further

430   investigation is certainly required, this would open up for completely new applications

431   of 14F7, in the clinical setting as well as for biochemical analysis.

432

433   **Conclusions**

434   We set out to characterize the exquisite specificity of 14F7 for NeuGc GM3, and its

435   selectivity over NeuAc GM3, and have now solved the crystal structure of this

436   promising anti-tumor antibody in complex with its target antigen by high-resolution X-

437   ray crystallography. Complementary qualitative and quantitative liposome interaction

438   studies with NeuGc GM3 additionally yielded unique insights into the formation and
439   characteristics of glycolipid clusters and, potentially, membrane nanodomains.

440   Generally, antigen and immunogen are thought to have identical structures. Our data
441   suggest that NeuGc GM3 concentration in the membrane influences its presentation
442   and, in consequence, strongly affects recognition by 14F7. Therefore, although the
443   immunogen is NeuGc GM3, the actual antigen recognized by 14F7 antibody is "high
444   density NeuGc GM3". Similar results were previously described for the M2590 mAb
445   for NeuAc GM3[64]. Here we show additionally that different gangliosides can
446   conformationally modulate each other, *i.e.*, the presence of NeuAc GM3 helps convert
447   NeuGc GM3 to its antigenic form. The switch between conformations appears to be
448   abrupt, as caused by a phase transition, at sufficiently high concentration. However,
449   binding requires that the membrane surface is relatively flat, as in GUVs and MLVs,
450   and probably in biological membranes. We suspect that high positive curvature may
451   disrupt the alignment of the saccharide head groups, abrogating binding of 14F7
452   (Figure 6). It may also dilute the concentration of negative charges, affecting
453   electrostatic membrane-antibody interactions.

454   Our findings further suggest that under favorable conditions, such as the presence of
455   interacting molecules like NeuAc GM3, NeuGc GM3 can be recognized even at
456   relatively low concentrations in cellular membranes, despite requirement of a "high-
457   density-form". Our data thus inform new concepts for designing new immunotherapy
458   strategies targeting glycolipids.

459

460 **Methods**

461 **Synthesis of NeuGc trisaccharide**

462 The NeuGc GM3 trisaccharide was synthesized through an IBr/AgOTf-promoted

463 glycosylation of a benzylated lactose acceptor with a NeuGc thioglycoside donor,

464 followed by global deprotection of the obtained trisaccharide as reported earlier[9].

465

466 **Expression and purification of 14F7 derived scFv**

467 The 14F7 scFv was produced by a variation of a protocol described by Bjerregaard-

468 Andersen *et al.*[9]. Compared to the original 14F7 mAb, this construct contains an

469 alternative light chain identified by Rojas *et al.*[8]. The linker was chosen on the basis of

470 a vector system established for expression of single chain T-cell receptors (TCRs) and

471 single-chain variable fragments (scFvs) in *Escherichia coli*[80,81]. Briefly, the scFv was

472 expressed in *E. coli* by a pFKPEN vector-based system. The vector encodes a pelB

473 leader sequence, thus promoting the translocation of the protein to the periplasm.

474 Purification included limited lysis of the *E. coli* outer membrane to release the mature

475 scFv, and subsequent purification by protein L affinity chromatography and size

476 exclusion chromatography to reach a highly pure and homogenous preparation for

477 crystallization and binding experiments.

478

479 **Crystallization of the 14F7 scFv in complex with NeuGc trisaccharide**

480 Crystallization of the 14F7 scFv was performed as described earlier[9]. Crystals of good

481 diffraction quality were obtained from the Morpheus screen (Hampton Research, US)

482 after seeding with small crystals from initial hits. Remaining crystals from the D12

483 condition (12.5 % w/v PEG 1000, 12.5 % w/v PEG 3350, 12.5 % v/v MPD, 0.02 M

484 1,6-hexanediol, 0.02 M 1-butanol, 0.02 M(*RS*)-1,2-propanediol, 0.02 M 2-propanol,

485 0.02 M 1,4-butanediol, 0.02 M 1,3-propanediol, 0.1 M Bicine/Tris base pH 8.5), used

486 for determination of the 14F7 scFv apo-structure[9], were soaked by the addition of the

487 synthesized NeuGc trisaccharide in powder form. The crystals were incubated for 1h

488 before flash-cooling in liquid nitrogen and stored for diffraction experiments.

489

Data collection and structure determination

Diffraction data extending to 2.3 Å were collected at the ID30A-3 beam line at the European Synchrotron Radiation Facility (ESRF), Grenoble, France. X-ray data were auto-processed at the ESRF by the EDNA pipeline[82]. The structure was phased by molecular replacement with the PHENIX crystallographic software package[83], using the 14F7 scFv apo-structure (PDB ID: 6FFJ[9]) as search model, and refined in alternating cycles of manual model building and refinement with PHENIX[83] and COOT[84]. Water molecules were built in at late stages of the refinement, initially using the automated finding by PHENIX. These sites were then inspected individually and assessed for removal in case of electron density sigma level >1.10 e/Å^3 or bond distances >3.5 Å or <2.2 Å. Likewise, missing water molecules were added manually. The phased map revealed additional electron density in one of the four scFv molecules in the asymmetric unit, which was modelled as NeuGc GM3 trisaccharide. The trisaccharide ligand was built using eLBOW[85] and modeled into the electron density of the binding pocket at final stages of structure building and adjusting occupancy by matching ligand *B*-factors to interacting protein residues. An OMIT difference density map was made by removing the trisaccharide ligand from the final model, followed by five refinement cycles using PHENIX[83] The final model was deposited in the Protein Data Bank with accession code 6S2I.

Modeling

The program VMD[86] was used to for visualization and analysis, as well as for molecular modeling. The two amino acid substitutions in the heavy variable domain – S31R and W33Q – were made using the Mutator plugin implemented in VMD. Side chain conformations were modeled using the Molefacture plugin. This same tool was used to model the anticlinal conformation of the GM3 trisaccharide, keeping the sialic acid in its crystal position and modifying only the two torsion angles of its glycosidic linkage with galactose.

Preparation of giant unilamellar vesicles (GUVs)

1,2-dioleoyl-*sn*-glycero-3-phosphocholine (DOPC) and cholesterol (both from Avanti, US) stocks were dissolved in chloroform/methanol (10:1), *N*-Acetyl (Matreya, US)

522 and/or *N*-glycolyl GM3 (isolated from horse erythrocytes[87] and kindly provided by

523 CIM, Havana, Cuba) were dissolved in chloroform/methanol/water (2:1:0.1). GUVs

524 were prepared by the polyvinyl alcohol (PVA; Mw 146,000-186,000, Sigma Aldrich,

525 Germany) assisted method in the absence of divalent ions. Black, 96-well glass bottom

526 plates (Greiner Bio-One) were coated with 2 % PVA and evaporated by heating at

527 70 °C for 20 min. In total 10 µl of desired lipid mixtures at 1 mg/mL in

528 chloroform/methanol/water 1/2/0.8 (v/v) was spread on top of the PVA coated wells,

529 followed by subsequent incubation under vacuum for at least 1 h to form a lipid film

530 and allow removal of organic solvents. Sucrose containing swelling buffer (280 mM

531 sucrose, 25 mM HEPES-NaOH, pH 7.4; 300 µl per well) was added and incubated for

532 at least 20 min to induce vesicle formation.

533

534 **Confocal imaging**

535 GUVs were deposited in a 1 % BSA precoated imaging chamber (384-Well Glass-

536 Bottom Plates, Greiner Bio-One, Austria). Labeled 14F7 mAb (14F7hT) was added and

537 the sample was left for 30 min incubation at 23 °C before confocal imaging. GUVs

538 were imaged with a Zeiss LSM 780 confocal microscope. 488 nm and 543 nm lasers

539 were used for excitation of green and red fluorophores, respectively. BP 530-550, BP

540 585-615 filters in multi-track mode were used to eliminate the cross talk.

541

542 **Preparation of liposomes**

543 For vesicle preparation, lipids (DOPC and cholesterol from Avanti, US, NeuAc GM3

544 from Matreya, US, and NeuGc GM3 from CIM, Havana, Cuba) were mixed at the

545 desired molar ratios and dried under nitrogen gas stream, followed by incubation under

546 vacuum for 4 h to remove organic solvents. The dried lipid film was re-hydrated in

547 HEPES-buffered saline (HBS) (10 mM HEPES -NaOH, 150 mM NaCl, pH 7.4) to a

548 final concentration of 1 mg/mL, for 15 min at 600 rpm. Multilamellar vesicles (MLV)

549 were either used directly or further processed to yield unilamellar vesicles (LUVs).

550 LUVs where produced by subjecting the liposomes to 10 cycles of freezing in liquid

551 nitrogen and subsequent thawing in a heating block at 30 °C. The vesicle solution was

552 extruded 21 times through a 100 nm diameter polycarbonate membrane (Whatman®

553 Nuclepore, Fisher Scientific, US) using an extrusion kit (Avanti, US). The size of the

554   liposomes was determined by dynamic light scattering using a Zetasizer Nano ZS

555   (Malvern Instruments, UK).

556

557   **Lipid extraction and validation by thin-layer chromatography (TLC)**

558   Lipid composition of liposomes was assayed by thin layer chromatography as described

559   previously[88]. Briefly, lipids were extracted using two step extraction protocol

560   (chloroform:methanol 10:1 followed by 2:1)[88]. After each step, the lipid containing

561   organic phase was pooled and dried under a nitrogen stream. The lipids were

562   resuspended in a small volume of chloroform/methanol (2:1) and applied to a to HPTLC

563   plate (Silica Gel 60, Merck, Germany) together with DOPC/cholesterol and

564   NeuGc/NeuAc GM3 as standards. The plate was placed under vacuum for 30 min. For

565   development, chloroform/methanol/ 0.2 % calcium chloride (60/35/6) was used. To

566   visualize glycolipids, the plate was sprayed with orcinol (Sigma Aldrich, Germany) and

567   heated (200 °C until desired signal was observed).

568

569   **Flotation assay**

570   50 µl of liposomes was mixed with 14F7 mAb (14F7hT) or scFv (20 µg/mL final

571   concentration) and incubated for 30 min on ice. Thereafter, iodixanol (Optiprep; Sigma

572   Aldrich, Germany) was added to a final concentration of 30 % and a step gradient was

573   built on top (10 %, 2.5 %, and 0 % iodixanol in HBS). Protein-liposome complexes

574   were separated from unbound protein by centrifugation (2 h at 45.000 rpm, 4 °C,

575   MLS50 rotor -Beckman Coulter) in the density gradient. After flotation, 11 fractions

576   were collected from top of the tube. Samples were precipitated with 10 % TCA and

577   pelleted by centrifugation (20 min, 20,000 x g, 4 °C). The supernatant was discarded,

578   and the remaining pellet was neutralized with 1.5 M Tris -HCl, pH 8.8. SDS loading

579   buffer (250 mM Tris-HCl pH 6.8, 12.5 mM EDTA, 10 % SDS, 25 % glycerol, 200 mM

580   DTT) was added to all samples before loading on a 4-12 % Bis-Tris gel for SDS-

581   electrophoresis.

582

583

584

585 **Electrochemiluminescence immunoassay (EIA)**

586 Liposomes were passively adsorbed on the electrode surface (1 h, 23 ℃), and the

587 residual sites on the surface were blocked with 0.2 % porcine gelatin (1 h, 23 ℃). The

588 surface was then washed three times with HBS and porcine gelatin solutions containing

589 the desired concentrations of 14F7 mAb or scFv (were added to each well). Binding

590 was carried out for 2 h at 23 ℃. Wells were then washed and a solution of goat anti-

591 human-SulfoTAG (Mesoscale Discovery, US) or protein L-SulfoTAG was added

592 (1 µg/mL, 23 ℃, 1 h). The wells were washed and reading buffer was added (MSD

593 surfactant-free reading buffer). The background was determined from binding of

594 secondary antibodies or protein L to liposomes. Data were acquired on a SECTOR

595 Imager 6000. The recorded data were analyzed using GraphPad Prism 6.0 software

596 using one site-specific binding algorithm.

597

598 **Labeling of humanized 14F7 mAb (14F7hT) and protein L**

599 14F7hT was labeled using the DyLight 488-NHS ester (Thermo Fisher, US) for

600 detection during confocal microscopy. Protein L was labeled with SulfoTAG-NHS

601 ester (Mesoscale Discovery, US) at a 1:20 molar ratio for scFv detection during EIA.

602 The mixture was incubated for 1 h at 4 °C. The reaction was stopped by the addition of

603 at least 5-fold molar excess of ethanolamine over the NHS-reagent, followed by the

604 removal of excess label-molecules by a gravity spin column (GE Healthcare, Germany).

605

606 **Thermal stability measurements using nanoDSF**

607 For nanoDSF measurements, scFv was diluted with HBS to reach a final concentration

608 of 0.5 mg/mL, and subsequently filled into nanoDSF standard treated capillaries.

609 Thermal unfolding and aggregation was monitored in a temperature ramp with 1 °C/min

610 from 20 °C to 95 °C with a resolution of ~ 20 data points/min. Analysis of unfolding

611 and aggregation was performed using the PR.Control Software.

612

613 **Surface Plasmon Resonance**

614 SPR experiments were performed using a BIAcore X100 instrument on an HPA sensor

615 chip[89] (GE Healthcare, Germany). An HPA chip was cleaned with 40 mM octyl-

616 glucoside (10 µL/min, 5 min). Next, LUVs consisting of DOPC, cholesterol (both from

617 Avanti, US), NeuGc GM3 (CIM, Havana, Cuba) and/or NeuAc GM3 (Matreya, US) at

618 the desired molar ratios, were injected across the sensor chip at a low flow rate. The

619 LUVs (400 µM) were allowed to collapse and form a monolayer on the HPA chip

620 (2 µL/min, 15 min). Then, the chip was washed twice with 10 M NaOH (10 µL/min,

621 30 s), and once with HBS (10 mM HEPES, 150 mM NaCl, pH 7.4) (80 ul/min, 60 s) to

622 remove any unbound liposomes. The end-response was between 900 and 1300 RU.

623 14F7 mAb (500 nM) in HBS was injected at 30 µL/min for 3 min. The dissociation

624 phase was measured for 5 min. At the end of the binding assay, the surface of the sensor

625 chip was regenerated with two injections of 3:2 10 M NaOH/isopropanol (10 µL/min,

626 30 s). The binding response of the 14F7 mAb was obtained after subtracting the binding

627 signal from the reference flow cell containing vesicles without gangliosides. The

628 experiment was repeated twice with similar results.

629

630 **Western blot**

631 Proteins were transferred to a 0.45 μm membranes (Millipore) for immunoblotting. The

632 membrane was incubated for 1 h on a tilting tray (10 rpm, 23 °C) in TM-PBS buffer

633 (0.1 % Tween 20, 5 % nonfat dry milk powder in 1x PBS), before a 20 sec wash in

634 fresh TM-PBS. Secondary antibody (Goat anti-human IgG, 1.25 μg/mL, SulfoTAG)

635 diluted in TM-PBS was added, and the membrane was incubated for 1 h (10 rpm,

636 23 °C). The membrane was washed thrice in 5 min intervals, twice in T-PBS (0.1 %

637 Tween 20 in 1x PBS) and once in 1x PBS. Detection was performed with a CCD imager

638 (Imager 600, GE Healthcare) using SuperSignal West Pico PLUS (Thermo Fisher, US)

639 as substrate.

640

Acknowledgements

Author contributions

H.J., M.G., Ü.C. and U.K. conceived the study. F.A. synthesized the trisaccharide, supervised by S.O.. H.J. expressed and purified the constructs, supervised by U.K.. K.B.-A. was in charge of the crystallography, with U.K. validating the crystal structure. E.M. performed the modeling studies. Liposome experiments were performed by H.J., D.G. and M.G., who also served as supervisor for this part of the work. SPR experiments were performed by H.J. and A.S., supervised by G.A.. K.B.-A. and H.J. wrote the first draft of the manuscript, which was revised in tight collaboration with E.M., M.G. and U.K., and approved by all authors.

References

674

675 1 Dennis, J. W., Laferté, S., Waghorne, C., Breitman, M. L. & Kerbel, R. S. β1-6
676 branching of Asn-linked oligosaccharides is directly associated with metastasis.
677 *Science* **236**, 582-585, doi:10.1126/science.2953071 (1987).

678 2 Hakomori, S. in *The molecular immunology of complex carbohydrates-2. Advances in*
679 *experimental medicine and biology* Vol. 491 (ed Albert M. Wu) Ch. Tumor-
680 associated carbohydrate antigens defining tumor malignancy: basis for development
681 of anti-cancer vaccines, 369-402 (Springer, Boston, MA, 2001).

682 3 Pochechueva, T., Jacob, F., Fedier, A. & Heinzelmann-Schwarz, V. Tumor-
683 associated glycans and their role in gynecological cancers: accelerating translational
684 research by novel high-throughput approaches. *Metabolites* **2**, 913-939,
685 doi:10.3390/metabo2040913 (2012).

686 4 Scott, A. M., Geleick, D., Rubira, M., Clarke, K., Nice, E. C., Smyth, F. E., Stockert,
687 E., Richards, E. C., Carr, F. J., Harris, W. J., Armour, K. L., Rood, J., Kypridis, A.,
688 Kronina, V., Murphy, R., Lee, F.-T., Liu, Z., Kitamura, K., Ritter, G., Laughton, K.,
689 Hoffman, E., Burgess, A. W. & Old, L. J. Construction, production, and
690 characterization of humanized anti-Lewis Y monoclonal antibody 3S193 for targeted
691 immunotherapy of solid tumors. *Cancer Res* **60**, 3254-3261 (2000).

692 5 Yu, A. L., Gilman, A. L., Ozkaynak, M. F., London, W. B., Kreissman, S. G., Chen,
693 H. X., Smith, M., Anderson, B., Villablanca, J. G., Matthay, K. K., Shimada, H.,
694 Grupp, S. A., Seeger, R., Reynolds, C. P., Buxton, A., Reisfeld, R. A., Gillies, S. D.,
695 Cohn, S. L., Maris, J. M. & Sondel, P. M. for the Children's Oncology Group. Anti-
696 GD2 antibody with GM-CSF, interleukin-2, and isotretinoin for neuroblastoma. *N*
697 *Engl J Med* **363**, 1324-1334, doi:10.1056/NEJMoa0911123 (2010).

698 6 Hutchins, L. F., Makhoul, I., Emanuel, P. D., Pennisi, A., Siegel, E. R., Jousheghany,
699 F., Guo, X., Pashov, A. D., Monzavi-Karbassi, B. & Kieber-Emmons, T. Targeting
700 tumor-associated carbohydrate antigens: a phase I study of a carbohydrate mimetic-
701 peptide vaccine in stage IV breast cancer subjects. *Oncotarget* **8**, 99161-99178,
702 doi:10.18632/oncotarget.21959 (2017).

703 7 Carr, A., Mullet, A., Mazorra, Z., Vázquez, A. M., Alfonso, M., Mesa, C., Rengifo,
704 E., Pérez, R. & Fernández, L. E. A mouse IgG1 monoclonal antibody specific for *N*-
705 glycolyl GM3 ganglioside recognized breast and melanoma tumors. *Hybridoma* **19**,
706 241-247, doi:10.1089/02724570050109639 (2000).

707 8 Rojas, G., Talavera, A., Munoz, Y., Rengifo, E., Krengel, U., Ångström, J.,
708 Gavilondo, J. & Moreno, E. Light-chain shuffling results in successful phage display
709 selection of functional prokaryotic-expressed antibody fragments to *N*-glycolyl GM3
710 ganglioside. *J Immunol Methods* **293**, 71-83, doi:10.1016/j.jim.2004.07.002 (2004).

711 9 Bjerregaard-Andersen, K., Johannesen, H., Abdel-Rahman, N., Heggelund, J. E.,
712 Hoås, H. M., Abraha, F., Bousquet, P. A., Høydahl, L. S., Burschowsky, D., Rojas,
713 G., Oscarson, S., Løset, G. Å. & Krengel, U. Crystal structure of an L chain
714 optimised 14F7 anti-ganglioside Fv suggests a unique tumour-specificity through an
715 unusual H-chain CDR3 architecture. *Sci Rep* **8**, 1-11, doi:10.1038/s41598-018-28918-
716 5 (2018).

717 10 Torbidoni, A. V., Scursoni, A., Camarero, S., Segatori, V., Gabri, M., Alonso, D.,
718 Chantada, G. & de Dávila, M. T. G. Immunoreactivity of the 14F7 Mab raised against
719 *N*-glycolyl GM3 ganglioside in retinoblastoma tumours. *Acta Ophthalmol* **93**, e294-
720 e300, doi:10.1111/aos.12578 (2015).

721 11 Blanco, R., Rengifo, C. E., Cedeño, M., Frómeta, M., Rengifo, E. & Carr, A.
722 Immunoreactivity of the 14F7 Mab (raised against N-glycolyl GM3 ganglioside) as a

723 positive prognostic factor in non-small-cell lung cancer. *Patholog Res Int* **2012**, 1-12,
724 doi:10.1155/2012/235418 (2012).

725 12 Lahera, T., Calvo, A., Torres, G., E Rengifo, C., Quintero, S., Arango, M. d. C.,
726 Danta, D., Vázquez, J. M., Escobar, X. & Carr, A. Prognostic role of 14F7 Mab
727 immunoreactivity against N-glycolyl GM3 ganglioside in colon cancer. *J Oncol* **2014**,
728 1-8, doi:10.1155/2014/482301 (2014).

729 13 Oliva, J. P., Valdés, Z., Casacó, A., Pimentel, G., González, J., Álvarez, I., Osorio,
730 M., Velazco, M., Figueroa, M., Ortiz, R., Escobar, X., Orozco, M., Cruz, J., Franco,
731 S., Díaz, M., Roque, L., Carr, A., Vázquez, A. M., Mateos, C., Rubio, M. C., Pérez,
732 R. & Fernández, L. E. Clinical evidences of GM3 (NeuGc) ganglioside expression in
733 human breast cancer using the 14F7 monoclonal antibody labelled with [99m]Tc. *Breast*
734 *Cancer Res and Treat* **96**, 115-121, doi:10.1007/s10549-005-9064-0 (2006).

735 14 Fernández-Marrero, Y., Roque-Navarro, L., Hernández, T., Dorvignit, D., Molina-
736 Pérez, M., González, A., Sosa, K., López-Requena, A., Pérez, R. & Mateo de Acosta,
737 C. A cytotoxic humanized anti-ganglioside antibody produced in a murine cell line
738 defective of *N*-glycolylated-glycoconjugates. *Immunobiology* **216**, 1239-1247,
739 doi:10.1016/j.imbio.2011.07.004 (2011).

740 15 Dorvignit, D., Boligan, K. F., Relova-Hernández, E., Clavell, M., López, A., Labrada,
741 M., Simon, H.-U., López-Requena, A., Mesa, C. & von Gunten, S. Antitumor effects
742 of the GM3(Neu5Gc) ganglioside-specific humanized antibody 14F7hT against
743 *Cmah*-transfected cancer cells. *Sci Rep* **9**, 1-12, doi:10.1038/s41598-019-46148-1
744 (2019).

745 16 Carr, A., Mesa, C., Arango, M. d. C., Vázquez, A. M. & Fernández, L. E. *In vivo* and
746 *in vitro* anti-tumor effect of 14F7 monoclonal antibody. *Hybrid Hybridomics* **21**, 463-
747 468, doi:10.1089/153685902321043990 (2002).

748 17 Roque-Navarro, L., Chakrabandhu, K., de León, J., Rodríguez, S., Toledo, C., Carr,
749 A., de Acosta, C. M., Hueber, A.-O. & Pérez, R. Anti-ganglioside antibody-induced
750 tumor cell death by loss of membrane integrity. *Mol Cancer Ther* **7**, 2033-2041,
751 doi:10.1158/1535-7163.MCT-08-0222. (2008).

752 18 Rojas, G., Pupo, A., Gómez, S., Krengel, U. & Moreno, E. Engineering the binding
753 site of an antibody against *N*-glycolyl GM3: from functional mapping to novel anti-
754 ganglioside specificities. *ACS Chem Biol* **8**, 376-386, doi:10.1021/cb3003754 (2013).

755 19 Krengel, U., Olsson, L.-L., Martínez, C., Talavera, A., Rojas, G., Mier, E., Ångström,
756 J. & Moreno, E. Structure and molecular interactions of a unique antitumor antibody
757 specific for *N*-glycolyl GM3. *J Biol Chem* **279**, 5597-5603,
758 doi:10.1074/jbc.M311693200 (2004).

759 20 Labrada, M., Dorvignit, D., Hevia, G., Rodríguez-Zhurbenko, N., Hernández, A. M.,
760 Vázquez, A. M. & Fernández, L. E. GM3(Neu5Gc) ganglioside: an evolution fixed
761 neoantigen for cancer immunotherapy. *Semin Oncol* **45**, 41-51,
762 doi:10.1053/j.seminoncol.2018.04.003 (2018).

763 21 Chou, H.-H., Takematsu, H., Diaz, S., Iber, J., Nickerson, E., Wright, K. L.,
764 Muchmore, E. A., Nelson, D. L., Warren, S. T. & Varki, A. A mutation in human
765 CMP-sialic acid hydroxylase occurred after the *Homo-Pan* divergence. *Proc Natl*
766 *Acad Sci U S A* **95**, 11751-11756, doi:10.1073/pnas.95.20.11751 (1998).

767 22 Irie, A., Koyama, S., Kozutsumi, Y., Kawasaki, T. & Suzuki, A. The molecular basis
768 for the absence of *N*-glycolylneuraminic acid in humans. *J Biol Chem* **273**, 15866-
769 15871, doi:10.1074/jbc.273.25.15866 (1998).

770 23 Varki, A. N-glycolylneuraminic acid deficiency in humans. *Biochimie* **83**, 615-622,
771 doi:10.1016/S0300-9084(01)01309-8 (2001).

772   24   Tangvoranuntakul, P., Gagneux, P., Diaz, S., Bardor, M., Varki, N., Varki, A. &
773   Muchmore, E. Human uptake and incorporation of an immunogenic nonhuman
774   dietary sialic acid. *Proc Natl Acad Sci U S A* **100**, 12045-12050,
775   doi:10.1073/pnas.2131556100 (2003).

776   25   Bardor, M., Nguyen, D. H., Diaz, S. & Varki, A. Mechanism of uptake and
777   incorporation of the non-human sialic acid *N*-glycolylneuraminic acid into human
778   cells. *J Biol Chem* **280**, 4228-4237, doi:10.1074/jbc.M412040200 (2005).

779   26   Byres, E., Paton, A. W., Paton, J. C., Löfling, J. C., Smith, D. F., Wilce, M. C.,
780   Talbot, U. M., Chong, D. C., Yu, H., Huang, S., Chen, X., Varki, N. M., Varki, A.,
781   Rossjohn, J. & Beddoe, T. Incorporation of a non-human glycan mediates human
782   susceptibility to a bacterial toxin. *Nature* **456**, 648-652, doi:10.1038/nature07428
783   (2008).

784   27   Banda, K., Gregg, C. J., Chow, R., Varki, N. M. & Varki, A. Metabolism of
785   vertebrate amino sugars with *N*-glycolyl groups: mechanisms underlying
786   gastrointestinal incorporation of the non-human sialic acid xeno-autoantigen *N*-
787   glycolylneuraminic acid. *J Biol Chem* **287**, 28852-28864,
788   doi:10.1074/jbc.M112.364182 (2012).

789   28   Dhar, C., Sasmal, A. & Varki, A. From «serum sickness» to «xenosialitis»: past,
790   present, and future significance of the non-human sialic acid Neu5Gc. *Front Immunol*
791   **10**, 1-16, doi:10.3389/fimmu.2019.00807 (2019).

792   29   Bremer, E. G., Schlessinger, J. & Hakomori, S. Ganglioside-mediated modulation of
793   cell growth. Specific effects of G_{M3} on tyrosine phosphorylation of the epidermal
794   growth factor receptor. *J Biol Chem* **261**, 2434-2440 (1986).

795   30   Hanai, N., Nores, G. A., MacLeod, C., Torres-Mendez, C.-R. & Hakomori, S.
796   Ganglioside-mediated modulation of cell growth. Specific effects of GM_3 and lyso-
797   GM_3 in tyrosine phosphorylation of the epidermal growth factor receptor. *J Biol*
798   *Chem* **263**, 10915-10921 (1988).

799   31   Kabayama, K., Sato, T., Saito, K., Loberto, N., Prinetti, A., Sonnino, S., Kinjo, M.,
800   Igarashi, Y. & Inokuchi, J. Dissociation of the insulin receptor and caveolin-1
801   complex by ganglioside GM3 in the state of insulin resistance. *Proc Natl Acad Sci U*
802   *S A* **104**, 13678-13683, doi:10.1073/pnas.0703650104 (2007).

803   32   Kawashima, N., Yoon, S.-J., Itoh, K. & Nakayama, K.-i. Tyrosine kinase activity of
804   epidermal growth factor receptor is regulated by GM3 binding through carbohydrate
805   to carbohydrate Interactions. *J Biol Chem* **284**, 6147-6155,
806   doi:10.1074/jbc.M808171200 (2009).

807   33   Coskun, Ü., Grzybek, M., Drechsel, D. & Simons, K. Regulation of human EGF
808   receptor by lipids. *Proc Natl Acad Sci U S A* **108**, 9044-9048,
809   doi:10.1073/pnas.1105666108 (2011).

810   34   Malykh, Y. N., Schauer, R. & Shaw, L. *N*-glycolylneuraminic acid in human
811   tumours. *Biochimie* **83**, 623-634, doi:10.1016/S0300-9084(01)01303-7 (2001).

812   35   Yin, J., Hashimoto, A., Izawa, M., Miyazaki, K., Chen, G.-Y., Takematsu, H.,
813   Kozutsumi, Y., Suzuki, A., Furuhata, K., Cheng, F.-L., Lin, C.-H., Sato, C., Kitajima,
814   K. & Kannagi, R. Hypoxic culture induces expression of sialin, a sialic acid
815   transporter, and cancer-associated gangliosides containing non–human sialic acid on
816   human cancer cells. *Cancer Res* **66**, 2937-2945 (2006).

817   36   Alisson-Silva, F., Kawanishi, K. & Varki, A. Human risk of diseases associated with
818   red meat intake: Analysis of current theories and proposed role for metabolic
819   incorporation of a non-human sialic acid. *Mol Aspects Med* **51**, 16-30,
820   doi:10.1016/j.mam.2016.07.002 (2016).

821   37   Bousquet, P. A., Sandvik, J. A., Jeppesen Edin, N. F. & Krengel, U. Hypothesis:
822   hypoxia induces *de novo* synthesis of NeuGc gangliosides in humans through CMAH
823   domain substitute. *Biochem Biophys Res Commun* **495**, 1562-1566,
824   doi:10.1016/j.bbrc.2017.11.183 (2018).

825   38   Siebert, H.-C., Reuter, G., Schauer, R., von der Lieth, C.-W. & Dabrowski, J.
826   Solution conformations of GM3 gangliosides containing different sialic acid residues
827   as revealed by NOE-based distance mapping, molecular mechanics, and molecular
828   dynamics calculations. *Biochemistry* **31**, 6962-6971, doi:10.1021/bi00145a014
829   (1992).

830   39   Simons, K. & van Meer, G. Lipid sorting in epithelial cells. *Biochemistry* **27**, 6197-
831   6202, doi:10.1021/bi00417a001 (1988).

832   40   Brown, D. A. & London, E. Structure and function of sphingolipid- and cholesterol-
833   rich membrane rafts. *J Biol Chem* **275**, 17221-17224, doi:10.1074/jbc.R000005200
834   (2000).

835   41   Pencer, J., Mills, T., Anghel, V., Krueger, S., Epand, R. M. & Katsaras, J. Detection
836   of submicron-sized raft-like domains in membranes by small-angle neutron
837   scattering. *Eur Phys J E Soft Matter* **18**, 447-458, doi:10.1140/epje/e2005-00046-5
838   (2005).

839   42   Lingwood, D. & Simons, K. Lipid rafts as a membrane-organizing principle. *Science*
840   **327**, 46-50, doi:10.1126/science.1174621 (2010).

841   43   Simons, K. & Sampaio, J. L. Membrane organization and lipid rafts. *Cold Spring
842   Harb Perspect Biol* **3**, 1-17, doi:10.1101/cshperspect.a004697 (2011).

843   44   Nickels, J. D., Chatterjee, S., Stanley, C. B., Qian, S., Cheng, X., Myles, D. A. A.,
844   Standaert, R. F., Elkins, J. G. & Katsaras, J. The in vivo structure of biological
845   membranes and evidence for lipid domains. *PLoS Biol* **15**, 1-22,
846   doi:10.1371/journal.pbio.2002214 (2017).

847   45   Semeraro, E. F., Devos, J. M., Porcar, L., Forsyth, V. T. & Narayanan, T. *In vivo*
848   analysis of the *Escherichia coli* ultrastructure by small-angle scattering. *IUCrJ* **4**,
849   751-757, doi:doi:10.1107/S2052252517013008 (2017).

850   46   Bremer, E. G., Hakomori, S., Bowen-Pope, D. F., Raines, E. & Ross, R. Ganglioside-
851   mediated modulation of cell growth, growth factor binding, and receptor
852   phosphorylation. *J Biol Chem* **259**, 6818-6825 (1984).

853   47   Hakomori, S. The glycosynapse. *Proc Natl Acad Sci U S A* **99**, 225-232,
854   doi:10.1073/pnas.012540899 (2002).

855   48   Klokk, T. I., Kavaliauskiene, S. & Sandvig, K. Cross-linking of glycosphingolipids at
856   the plasma membrane: consequences for intracellular signaling and traffic. *Cell Mol
857   Life Sci* **73**, 1301-1316, doi:10.1007/s00018-015-2049-1 (2016).

858   49   Cheng, X. & Smith, J. C. Biological membrane organization and cellular signaling.
859   *Chem Rev* **119**, 5849-5880, doi:10.1021/acs.chemrev.8b00439 (2019).

860   50   Krengel, U. & Bousquet, P. A. Molecular recognition of gangliosides and their
861   potential for cancer immunotherapies. *Front Immunol* **5**, 1-11,
862   doi:10.3389/fimmu.2014.00325 (2014).

863   51   Gierszal, K. P., Davis, J. G., Hands, M. D., Wilcox, D. S., Slipchenko, L. V. & Ben-
864   Amotz, D. π-hydrogen bonding in liquid water. *Phys Chem Lett* **2**, 2930-2933,
865   doi:10.1021/jz201373e (2011).

866   52   Peng, H.-P., Lee, K. H., Jian, J.-W. & Yang, A.-S. Origins of specificity and affinity
867   in antibody–protein interactions. *Proc Natl Acad Sci U S A* **111**, E2656-2665,
868   doi:10.1073/pnas.1401131111 (2014).

869   53   Durec, M., Marek, R. & Kozelka, J. Water–tryptophan interactions: lone-pair···π or
870   O–H···π? Molecular dynamics simulations of β-galactosidase suggest that both modes
871   can co-exist. *Chemistry* **24**, 5849-5859, doi:10.1002/chem.201705364 (2018).

872   54   Levy, Y. & Onuchic, J. N. Water mediation in protein folding and molecular
873   recognition. *Annu Rev Biophys Biomol Struct* **35**, 389-415,
874   doi:10.1146/annurev.biophys.35.040405.102134 (2006).

875   55   Bellissent-Funel, M.-C., Hassanali, A., Havenith, M., Henchman, R., Pohl, P.,
876   Sterpone, F., van der Spoel, D., Xu, Y. & Garcia, A. E. Water determines the
877   structure and dynamics of proteins. *Chem Rev* **116**, 7673-7697,
878   doi:10.1021/acs.chemrev.5b00664 (2016).

879   56   Weis, W. I. & Drickamer, K. Structural basis of lectin-carbohydrate recognition.
880   *Annu Rev Biochem* **65**, 441-473, doi:10.1146/annurev.bi.65.070196.002301 (1996).

881   57   Janin, J. Wet and dry interfaces: the role of solvent in protein–protein and protein–
882   DNA recognition. *Structure* **7**, R277-279, doi:10.1016/s0969-2126(00)88333-1
883   (1999).

884   58   Holmner, Å., Lebens, M., Teneberg, S., Ångström, J., Ökvist, M. & Krengel, U.
885   Novel binding site identified in a hybrid between cholera toxin and heat-labile
886   enterotoxin: 1.9 Å crystal structure reveals the details. *Structure* **12**, 1655-1667,
887   doi:10.1016/j.str.2004.06.022 (2004).

888   59   Braden, B. C., Fields, B. A. & Poljak, R. J. Conservation of water molecules in an
889   antibody–antigen interaction. *J Mol Recognit* **8**, 317-325, doi:10.1002/jmr.300080505
890   (1995).

891   60   Cohen, G. H., Silverton, E. W., Padlan, E. A., Dyda, F., Wibbenmeyer, J. A., Willson,
892   R. C. & Davies, D. R. Water molecules in the antibody–antigen interface of the
893   structure of the Fab HyHEL-5-lysozyme complex at 1.7 Å resolution: comparison
894   with results from isothermal titration calorimetry. *Acta Crystallogr D Biol*
895   *Crystallogr* **61**, 628-633, doi:10.1107/s0907444905007870 (2005).

896   61   Marino, S. F., Olal, D. & Daumke, O. A complex water network contributes to high–
897   affinity binding in an antibody–antigen interface. *Data Brief* **6**, 394-397,
898   doi:10.1016/j.dib.2015.12.023 (2015).

899   62   Horita, S., Nomura, Y., Sato, Y., Shimamura, T., Iwata, S. & Nomura, N. High-
900   resolution crystal structure of the therapeutic antibody pembrolizumab bound to the
901   human PD-1. *Sci Rep* **6**, 1-8, doi:10.1038/srep35297 (2016).

902   63   Yu, X., Coulson, B. S., Fleming, F. E., Dyason, J. C., von Itzstein, M. & Blanchard,
903   H. Novel structural insights into rotavirus recognition of ganglioside glycan receptors.
904   *J Mol Biol* **413**, 929-939, doi:10.1016/j.jmb.2011.09.005 (2011).

905   64   Nores, G. A., Dohi, T., Taniguchi, M. & Hakomori, S. Density-dependent recognition
906   of cell surface GM3 by a certain anti-melanoma antibody, and GM3 lactone as a
907   possible immunogen: requirements for tumor-associated antigen and immunogen. *J*
908   *Immunol* **139**, 3171-3176 (1987).

909   65   Stewart, R. J. & Boggs, J. M. A carbohydrate–carbohydrate interaction between
910   galactosylceramide–containing liposomes and cerebroside sulfate-containing
911   liposomes: dependence on the glycolipid ceramide composition. *Biochemistry* **32**,
912   10666-10674, doi:10.1021/bi00091a017 (1993).

913   66   Sezgin, E., Levental, I., Grzybek, M., Schwarzmann, G., Mueller, V., Honigmann, A.,
914   Belov, V. N., Eggeling, C., Coskun, Ü., Simons, K. & Schwille, P. Partitioning,
915   diffusion, and ligand binding of raft lipid analogs in model and cellular plasma

916   membranes. *Biochim Biophys Acta* **1818**, 1777-1784,
917   doi:10.1016/j.bbamem.2012.03.007 (2012).

918   67   Bolmatov, D., Soloviov, D., Zhernenkov, M., Zav'yalov, D., Mamontov, E., Suvorov,
919   A., Cai, Y. Q. & Katsaras, J. Molecular picture of the transient nature of lipid rafts.
920   *Langmuir* **36**, 4887-4896, doi:10.1021/acs.langmuir.0c00125 (2020).

921   68   Collard, L., Perez-Guaita, D., Faraj, B. H. A., Wood, B. R., Wallis, R., Andrew, P. W.
922   & Hudson, A. J. Light scattering by optically-trapped vesicles affords unprecedented
923   temporal resolution of lipid-raft dynamics. *Sci Rep* **7**, 1-11, doi:10.1038/s41598-017-
924   08980-1 (2017).

925   69   Kollmitzer, B., Heftberger, P., Rappolt, M. & Pabst, G. Monolayer spontaneous
926   curvature of raft-forming membrane lipids. *Soft Matter* **9**, 10877-10884,
927   doi:10.1039/c3sm51829a (2013).

928   70   Meinhardt, S., Vink, R. L. C. & Schmid, F. Monolayer curvature stabilizes nanoscale
929   raft domains in mixed lipid bilayers. *Proc Natl Acad Sci U S A* **110**, 4476-4481,
930   doi:10.1073/pnas.1221075110 (2013).

931   71   Sadeghi, S., Müller, M. & Vink, R. L. C. Raft formation in lipid bilayers coupled to
932   curvature. *Biophys J* **107**, 1591-1600, doi:10.1016/j.bpj.2014.07.072 (2014).

933   72   Seddon, J. M. & Templer, R. H. in *Handbook of Biological Physics. Structure and*
934   *dynamics of membranes: from cells to vesicles* Vol. 1 (eds R. Lipowsky & E.
935   Sackmann) Ch. 3. Polymorphism of lipid water systems, 97-160 (Elsevier Science
936   B.V., 1995).

937   73   Ipsen, J. H., Karlström, G., Mourtisen, O. G., Wennerström, H. & Zuckermann, M. J.
938   Phase equilibria in the phosphatidylcholine-cholesterol system. *Biochim Biophys Acta*
939   *Biomembr* **905**, 162-172, doi:10.1016/0005-2736(87)90020-4 (1987).

940   74   Ipsen, J. H., Mouritsen, O. G. & Zuckermann, M. J. Theory of thermal anomalies in
941   the specific heat of lipid bilayers containing cholesterol. *Biophys J* **56**, 661-667,
942   doi:10.1016/S0006-3495(89)82713-4 (1989).

943   75   Pascher, I. Molecular arrangements in sphingolipids. Conformation and hydrogen
944   bonding of ceramide and their implication on membrane stability and permeability.
945   *Biochim Biophys Acta Biomembr* **455**, 433-451, doi:10.1016/0005-2736(76)90316-3
946   (1976).

947   76   Nyholm, P.-G., Pascher, I. & Sundell, S. The effect of hydrogen bonds on the
948   conformation of glycosphingolipids. Methylated and unmethylated cerebroside
949   studied by X-ray single crystal analysis and model calculations. *Chem Phys Lipids* **52**,
950   1-10, doi:10.1016/0009-3084(90)90002-9 (1990).

951   77   DeMarco, M. L. & Woods, R. J. Atomic-resolution conformational analysis of the
952   G_{M3} ganglioside in a lipid bilayer and its implications for ganglioside–protein
953   recognition at membrane surfaces. *Glycobiology* **19**, 344-355,
954   doi:10.1093/glycob/cwn137 (2009).

955   78   Yahi, N., Aulas, A. & Fantini, J. How cholesterol constrains glycolipid conformation
956   for optimal recognition of Alzheimer's β amyloid peptide ($A_{β1-40}$). *PloS One* **5**, 9079-
957   9079, doi:10.1371/journal.pone.0009079 (2010).

958   79   Giri, R. P., Chakrabarti, A. & Mukhopadhyay, M. K. Cholesterol-induced structural
959   changes in saturated phospholipid model membranes revealed through X-ray
960   scattering technique. *J Phys Chem B* **121**, 4081-4090, doi:10.1021/acs.jpcb.6b12587
961   (2017).

962   80   Løset, G. Å., Løbersli, I., Kavlie, A., Stacy, J. E., Borgen, T., Kausmally, L.,
963   Hvattum, E., Simonsen, B., Hovda, M. B. & Brekke, O. H. Construction, evaluation

964   and refinement of a large human antibody phage library based on the IgD and IgM
965   variable gene repertoire. *J Immunol Methods* **299**, 47-62,
966   doi:10.1016/j.jim.2005.01.014 (2005).

967   81   Gunnarsen, K. S., Lunde, E., Kristiansen, P. E., Bogen, B., Sandlie, I. & Løset, G. Å.
968   Periplasmic expression of soluble single chain T cell receptors is rescued by the
969   chaperone FkpA. *BMC Biotechnol* **10**, 1-13, doi:10.1186/1472-6750-10-8 (2010).

970   82   Incardona, M.-F., Bourenkov, G. P., Levik, K., Pieritz, R. A., Popov, A. N. &
971   Svensson, O. *EDNA*: a framework for plugin-based applications applied to X-ray
972   experiment online data analysis. *J Synchrotron Radiat* **16**, 872-879,
973   doi:10.1107/s0909049509036681 (2009).

974   83   Adams, P. D., Afonine, P. V., Bunkóczi, G., Chen, V. B., Davis, I. W., Echols, N.,
975   Headd, J. J., Hung, L.-W., Kapral, G. J., Grosse-Kunstleve, R. W., McCoy, A. J.,
976   Moriarty, N. W., Oeffner, R., Read, R. J., Richardson, D. C., Richardson, J. S.,
977   Terwilliger, T. C. & Zwart, P. H. *PHENIX*: a comprehensive Python-based system for
978   macromolecular structure solution. *Acta Crystallogr D Biol Crystallogr* **66**, 213-221,
979   doi:10.1107/S0907444909052925 (2010).

980   84   Emsley, P., Lohkamp, B., Scott, W. G. & Cowtan, K. Features and development of
981   *Coot*. *Acta Crystallogr D Biol Crystallogr* **66**, 486-501,
982   doi:10.1107/S0907444910007493 (2010).

983   85   Moriarty, N. W., Grosse-Kunstleve, R. W. & Adams, P. D. *electronic Ligand Builder*
984   *and Optimization Workbench* (*eLBOW*): a tool for ligand coordinate and restraint
985   generation. *Acta Crystallogr D Biol Crystallogr* **65**, 1074-1080,
986   doi:10.1107/S0907444909029436 (2009).

987   86   Humphrey, W., Dalke, A. & Schulten, K. VMD: visual molecular dynamics. *J Mol*
988   *Graph* **14**, 33-38, 27-38, doi:10.1016/0263-7855(96)00018-5 (1996).

989   87   Folch, J., Arsove, S. & Meath, J. A. Isolation of brain strandin, a new type of large
990   molecule tissue component. *J Biol Chem* **191**, 819-831 (1951).

991   88   Ejsing, C. S., Sampaio, J. L., Surendranath, V., Duchoslav, E., Ekroos, K., Klemm, R.
992   W., Simons, K. & Shevchenko, A. Global analysis of the yeast lipidome by
993   quantitative shotgun mass spectrometry. *Proc Natl Acad Sci U S A* **106**, 2136-2141,
994   doi:10.1073/pnas.0811700106 (2009).

995   89   Šakanovič, A., Hodnik, V. & Anderluh, G. Surface plasmon resonance for measuring
996   Interactions of proteins with lipids and lipid membranes. *Methods Mol Biol* **2003**, 53-
997   70, doi:10.1007/978-1-4939-9512-7_3 (2019).

998

Supplementary Information
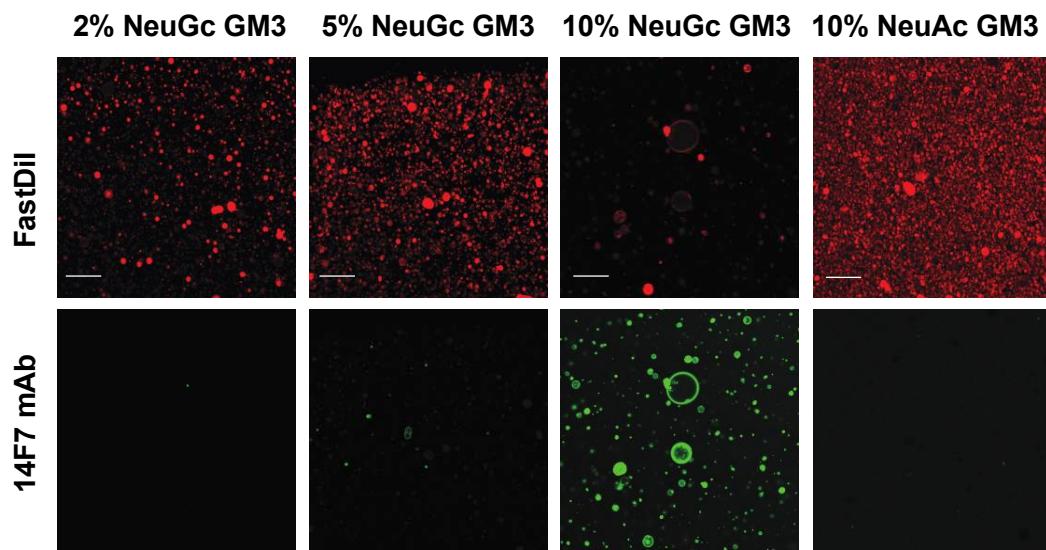
Figure S1. **Binding of 14F7 to GUVs composed of DOPC/Chol/GM3.** 14F7 was chemically labeled with Dylight-488 (green) and added to GUVs containing FastDiI as a membrane marker (red). While there was negligible interaction between 14F7 mAb and GUVs with 2 % and 5 % NeuGc GM3, 14F7 bound strongly to GUVs containing 10 % NeuGc GM3. No 14F7 mAb binding was observed for GUVs with 10 % NeuAc GM3. The scale bar corresponds to 20 μm.
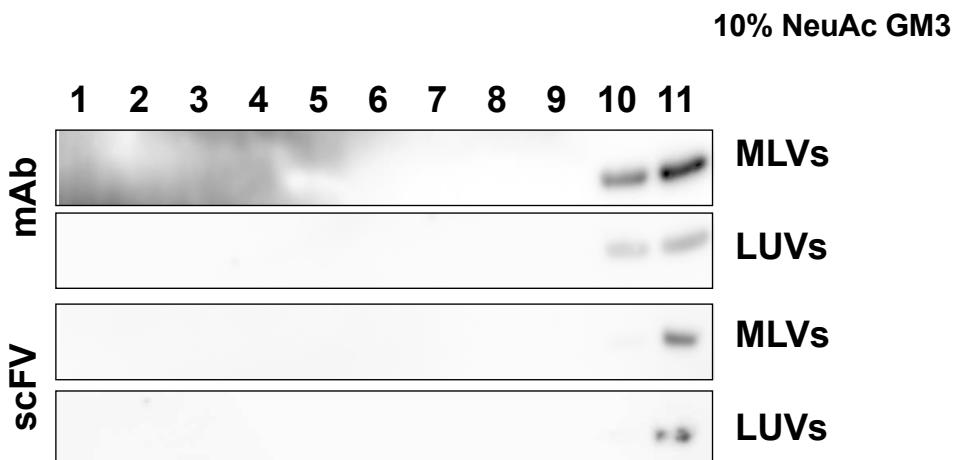
Figure S2. **Binding of 14F7 to LUVs and MLVs composed of 10 % NeuAc GM3/DOPC/ cholesterol in a flotation assay.** After centrifugation, 11 fractions were collected from the top. Proteins bound to vesicles accumulated in fractions 2-4. For all flotation assays with 10 % NeuAc GM3, the protein was located in the bottom fractions (10-11), where unbound proteins accumulate.
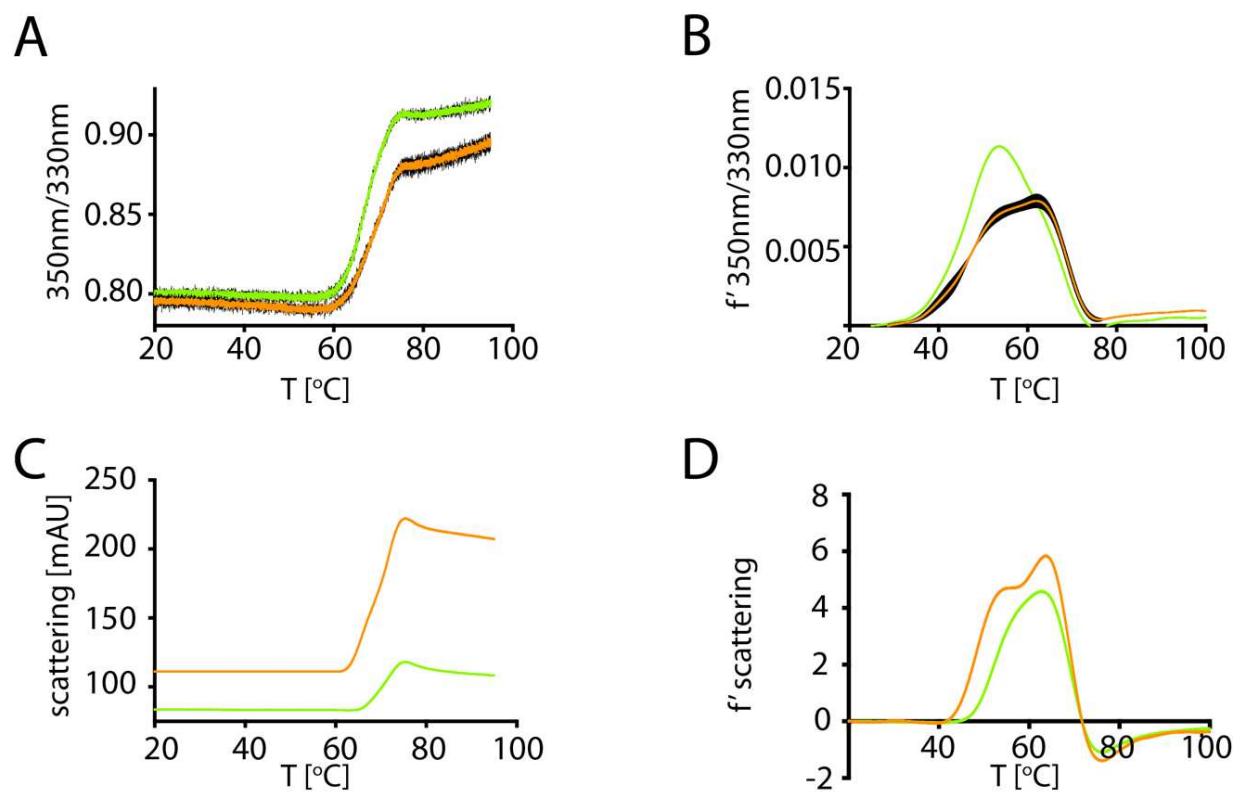
Figure S3. **nanoDSF measurements of native (green) and Dylight488-labeled (orange) 14F7 scFv.**
A Thermal unfolding curves. **B** First derivative of unfolding curves. **C** Aggregation propensity curves.
D First derivative of aggregation propensity curves.